Progress in Oceanography 219 (2023) 103159

Contents lists available at ScienceDirect

Progress in Oceanography

journal homepage: www.elsevier.com/locate/pocean

Environmental controls on macrozooplankton and fish distributions over diurnal to seasonal time scales in the northern Barents Sea

Heather Cannaby [a,*], Randi B. Ingvaldsen [a], Øyvind Lundesgaard [b], Angelika H.H. Renner [c], Georg Skaret [a], Serdar S. Sakinan [d], Terje Hovland [a], Melissa Chierici [c], Harald Gjøsæter [c]

[a] Institute of Marine Research, Nordnes, B.O. Box 1870, 5817 Bergen, Norway
[b] Norwegian Polar Institute, Fram Centre, Hjalmar Johansens gate 14, 9007, Norway
[c] Institute of Marine Research, Fram Centre, Hjalmar Johansens gate 14, 9007 Tromsø, Norway
[d] Wageningen Marine Research (WMR), 1976 CP Ijmuiden, The Netherlands

ARTICLE INFO

keywords:
Northern Barents Sea
Acoustic observations
Sound scattering layers
Temporal variability
Seasonality
Macrozooplankton
Nansen Legacy

ABSTRACT

We present acoustic observations obtained by bottom mounted echosounders at two locations in the northern Barents Sea and a third on the northern continental slope of the Barents Sea. Data collected over a period of approximately two years reveal significant variability in the density and depth distribution of pelagic macrozooplankton and fish. Variability over diurnal to seasonal timescales is related to light conditions, prevailing currents, water column characteristics (temperature, stability, and pycnocline depth) and to sea ice conditions. Of particular importance is the relative volume of Polar Water and Atlantic influenced water present at the mooring sites. On the northern continental shelf, above average concentrations of macrozooplankton and fish were observed during late summer and early autumn following ice melt, and during winter. Minimum densities of macrozooplankton and fish were observed during spring and early summer. These data demonstrate the persistent presence of a macrozooplankton community throughout the winter months in the northern Barents Sea. On the Great Bank full depth diel vertical migrations were observed throughout the Polar Night and under sea ice. At the two more northerly stations the density of the sound scattering layers performing diel vertical migrations and the vertical range of the migrations was greatest during the transition period between the polar night and mid-night sun periods. Superimposed on the seasonal variability in density distribution was significant shorter-term variability driven by hydrographic processes occurring over synoptic time scales. Significant mixing events, or changes in the prevailing current direction that lead to a change in water mass characteristics, forced changes in the concentration and depth distribution of macrozooplankton over periods of hours that were on occasion of similar magnitude to the seasonal variability. On the northern continental slope, a mesopelagic sound scattering layer more than 300 m thick at its seasonal maximum, was located for most of the year within the warm core of the Atlantic Water Boundary Current, ascending into the epipelagic zone for 5–6 weeks during summer. The density and thickness of this sound scattering layer were greatest during the late summer/early autumn and lowest during early spring. Fish-like scatterers were present, concentrated within the deeper regions of the sound scattering layer, during the winter months and during July.

1. Introduction

The Barents Sea is characterised by two distinct hydrographic domains, separated by the Polar Front (e.g., Loeng, 1991; Oziel et al., 2016). South of the Polar Front, warm and saline Atlantic Water (AW) occupies the entire water column (Fig. 1) and keeps the region ice free (e.g., Loeng, 1991; Ingvaldsen and Loeng, 2009). North of the Polar Front, the upper water column is generally comprised of cold and relatively fresh Polar Water (PW), and there is seasonal sea ice cover. The distribution of pelagic biota in the Barents Sea reflects water mass distributions, with substantial differences in food web structure and species composition on either side of the Polar Front (Kortsch et al., 2015; Kortsch et al., 2019; Van Engeland et al., 2023). The northern Barents Sea is characterized by a higher fraction of Arctic biota, adapted to sea ice cover, low temperatures and strong seasonality, while the southern Barents Sea is colonised by a higher fraction of boreal species.

* Corresponding author.
E-mail address: heather.anne.cannaby@hi.no (H. Cannaby).

https://doi.org/10.1016/j.pocean.2023.103159

Available online 3 November 2023

Intrusions of warm Atlantic influenced water into the northern Barents Sea bring with them Atlantic species which alter the local pelagic community composition (Dalpadado et al., 2012; Basedow et al., 2018). However, knowledge on the northern Barents Sea ecosystem is mostly based on summer data, and information about seasonality and biological activity during winter in this ice-covered region is limited.

The northern Barents Sea has experienced rapid warming throughout the water column, decreased sea ice import, and weakened stratification since 2005 (Lind et al., 2018), with warming attributed to a warmer, and possibly stronger inflow of sub-Arctic AW, which is expanding northwards (Asbjørnsen et al., 2020; Lind et al., 2018). This progression of AW into regions previously dominated by polar water, termed Atlantification, has resulted in an expansion of the range of boreal species, particularly along AW inflow pathways. Borealization has been observed at all trophic levels, with reported northward expansions of plankton (Lewis et al., 2020), demersal fish (Fossheim et al., 2015; Frainer et al., 2017) and sea mammals and seabirds (ICES, 2021). Sympagic organisms and organisms associated with the ice edge, on the other hand, are becoming less abundant due to sea ice retreat (Grémillet et al., 2015; Ershova et al., 2021).

The Barents Sea experiences large multiannual and multidecadal scale variability in sea ice conditions and water column characteristics (Sandø et al., 2010; Smedsrud et al., 2013). This results in strong interannual variability in the timing and duration of the short productive season. Adaptations to this uncertainty in seasonal production have been reported at both the individual level (e.g., through the plasticity in lifecycles and feeding strategies reported in copepod communities; (Kohlbach et al., 2021), and at a community level through low-connectivity and adaptable diets (Dolgov et al., 2021). Atlantification may impact both the timing of production and the nutritional quality of the phytoplankton as the community composition changes (Leu et al., 2010; Ji et al., 2010). Lipid-rich zooplankton (copepods, euphausiids, amphipods) form a key link in the transferal of energy up the food chain to species such as capelin, polar cod and whales in the Barents Sea (Dolgov et al., 2021). Warming of the Barents Sea is associated with a shift towards smaller boreal zooplankton species (e.g. Skjoldal et al., 2022 and references therein), the impact of which is unknown, but is likely to have consequences for the entire food chain.

The Barents Sea has been monitored extensively for over half a century with annual hydrographic surveys since the 1960s but sampling in the northern Barents Sea has been largely limited to the ice-free period during late summer and early autumn. This is particularly true for observations of zooplankton and fish, which have traditionally relied on ship-borne scientific echosounders supported by net sampling. Such surveys necessarily aim to cover the spatial area of interest in the shortest possible time and lack temporal detail. As ship-borne surveys alone cannot provide data on the time varying nature of organism concentrations, seasonal and shorter-term variability remains largely unknown.

Scattering layers in the epipelagic (<200 m) and mesopelagic (>200 m) zones, comprising aggregations of zooplankton and pelagic fish, are ubiquitous in most world oceans (Hays, 2003; Irigoien et al., 2014), and earlier studies have demonstrated such layers also exist in the Barents Sea (Ressler et al., 2015). Sound scattering layers detected by echosounders often rise at dusk and descend at dawn, due to the synchronous Diel Vertical Migration (DVM) of pelagic organisms. DVM is a common behavioural response believed to maximise feeding efficiency while minimising predation risk by visual predators in the upper water column (e.g. Hays, 2003). DVM is triggered by multiple exogeneous environmental cues, with daylight being the most important. DVM has, however, been observed in low light environments in the high Arctic during the polar night (Berge et al., 2009; Kraft et al., 2013). Acoustic moorings equipped with ADCPs and echosounders (e.g., Lee et al., 2004; Brierley et al., 2006; Velasco et al., 2018) allow assessment of temporal variability in the density distribution of sound scattering organisms. When such instruments are deployed alongside hydrographic moorings it becomes possible to interpret biophysical interactions over sub-hourly to seasonal timescales. The overarching aim of this study is to describe the seasonal and shorter-term variability in the density distribution of macrozooplankton and fish along AW advective pathways in the northern Barents Sea and on its northern continental slope. We aim to interpret this variability through analysis of the dominant physical drivers shaping the pelagic environment: sea ice conditions, day length, water mass characteristics and water column stratification. We utilise an array of moorings deployed as part of the Nansen Legacy project's observational programme which included bottom-mounted multi-frequency echosounders deployed along-side moorings collecting a range of physical and chemical data.

2. Methods

2.1. Study site

AW is transported from the Nordic Seas into the Arctic Ocean via two

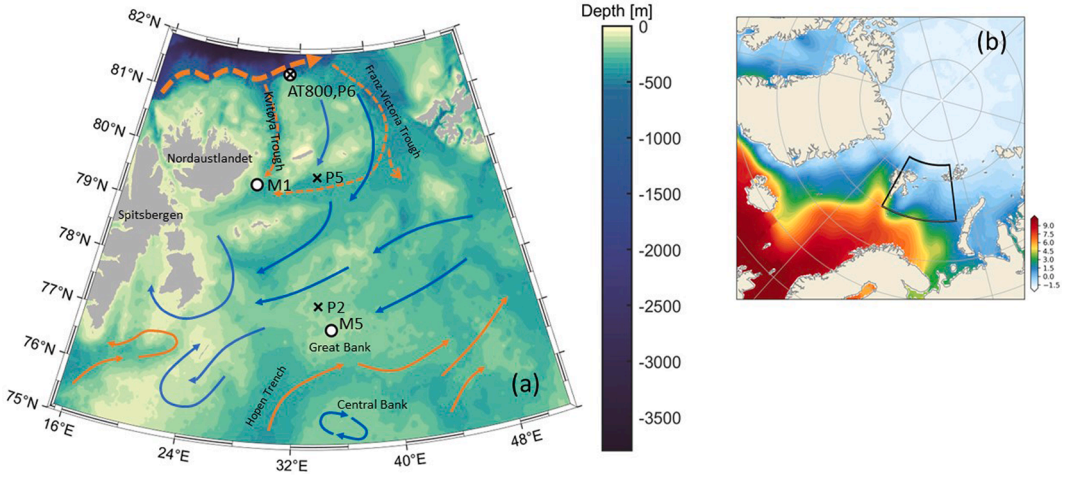

Redrawn from Eriksen et al. (2020) and Øyvind et al. (2022)

Fig. 1. (a) Bathymetric map of the Northern Barents Sea showing the Signature100 mooring locations (M5, M1 and AT800) and midwater ring net sampling stations (P2, P5 and P6). Red arrows indicate inflows of Atlantic Water or Atlantic influenced Water (solid arrows represent surface flow and dashed arrows subsurface flow). Blue arrows represent Polar Water. (b) Map of Arctic Ocean showing the location of the subdomain in (a), overlain by surface temperature climatology (WOA18 2005–2017 annual surface temperature climatology; Boyer et al., 2018).

main routes, through the Barents Sea and through the Fram Strait. AW enters the Barents Sea from the west through the Barents Sea Opening and spreads out within the Barents Sea, filling the region south of the Polar Front. The AW mixes with local water masses, cooling substantially, before entering the Arctic Ocean, largely via the St. Anna Trough in the Kara Sea (Fig. 1). AW is also transported northward via the West Spitsbergen Current. North of Svalbard, a fraction of the West Spitsbergen current turns eastwards and continues along the continental slope of the Nansen Basin (Pnyushkov et al., 2015; Våge et al., 2016), forming the Atlantic Water Boundary Current (AWBC). The AWBC plays an important role in regulating conditions in the eastern Arctic Ocean. A small fraction of the AW carried eastwards by the AWBC enters the northern Barents Sea primarily via two deep (>250 m) troughs: the wide Franz-Victoria Trough and the narrower Kvitøya Trough (Fig. 1; Lundesgaard et al., 2022; Matishov et al., 2009; Aksenov et al., 2010; Lind and Ingvaldsen, 2012).

AW in the northern Barents Sea is typically isolated from the surface (and hence sea ice) by strong stratification, appearing as a subsurface temperature maximum typically found at ~150–250 m depth (Lind et al., 2016). The strength of the ocean stratification in the northern Barents Sea depends both on the inflows of Polar Water (PW) and Warm Polar Water (wPW), and on the amount of sea ice that melts in the area (Lind et al., 2018). Increased meltwater input results in a fresher surface layer and strengthened vertical stratification. Stronger stratification limits the potential for vertical mixing and hence the upward flux of heat from the underlying AW layer, impacting ocean–atmosphere heat fluxes and sea ice formation over seasonal time scales (Lind et al., 2016).

Water masses in the study region have been defined here following Sundfjord et al. (2020). PW is defined as having a conservative temperature of less than 0 °C and a potential density of less than 27.97 kg m^{-3}. PW is typical of the upper water column in the northern Barents Sea and is characteristically formed by the introduction of (cold) sea ice melt water. wPW is formed either through the solar heating of PW or through mixing between AW or modified AW (mAW) and PW. wPW is defined as having a conservative temperature of more than 0 °C and an absolute salinity of less than 35.06 g kg^{-1}. mAW is defined as having a conservative temperature between 0.0 °C and 2.0 °C, and an absolute salinity more than or equal to 35.06 g kg^{-1}.

2.2. Acoustic moorings

Two submerged moorings were deployed in the northern Barents Sea, and a third was located on the continental slope north-east of Svalbard (Fig. 1). The moorings were equipped with Nortek Signature100s which combine a four-beam ADCP operating at 100 kHz and a central beam with a 70–120 kHz echosounder. Both the ADCP and the echosounder have an operational range of 300–400 m (Velasco et al., 2018). The Signature100s were also equipped with a thermometer and pressure sensor. The Signature100s were mounted in the centre of a mooring buoy, and oriented with transducers facing upward toward the water surface. Each mooring was in place for two consecutive deployments within the period August 2019 to November 2021. The individual mooring deployments are referred to as, e.g., *M1-Bio-1* (M1-Biological mooring, first deployment). In total we present approximately 2 years of data from each site, although at mooring site *M1-bio* there is a 5-month gap spanning winter 2020–21 (Table 1).

Fig. 1 shows the mooring locations overlain on a bathymetric map of the northern Barents Sea. Mooring *M1-bio* was located at a site of sloping bathymetry off the east coast of Nordaustlandet (Svalbard) at a depth of 259 m. This mooring was placed to capture AW inflow entering the Barents Sea from the north through the Kvitøya Trough. Mooring *M5-bio* was located in a fisheries protected area on the Great Bank, located at a depth of 147 m (later moved to 144 m). It was placed to capture organisms within the Polar Water present at this location, just north of the Polar Front (Våge et al., 2016). At both *M1-Bio* and *M5-bio,* the Signature100s were situated between 4 and 10 m above the seabed and recorded data from 2 m above the instrument depth (the echo-sounder blanking depth) up to within 2 m of the water surface (depending on surface conditions). The *AT800-bio* moorings were deployed on the continental slope north of Svalbard, located just east of the entrance to the Kvitøya Trough where they were intended to capture organisms transported eastwards by the AWBC. The *AT800-bio-1* mooring was deployed in a water depth of 876 m with the instrument located in the middle of the water column at 400 m depth. The *AT800-bio-2* mooring was located in a similar water depth (872 m), with the instrument installed at 453 m depth. In practice it was often difficult to obtain good data from the echosounder beyond a range of approximately 250–300 m, meaning the upper portion of the water column at *AT800* is not well resolved in the echosounder data. Full details of each mooring

Table 1
Mooring details. Abbreviations for measurements are as follows: T (temperature), C (Conductivity), S (salinity), P (pressure), DO (dissolved oxygen).

Mooring	Latitude (°N)	Longitude (°E)	Duration	Bottom Depth (m)	Median instrument Depth(s) (m)	Instruments	Echosounder Calibrated
Biology moorings							
M1-bio-1	79.589	28.091	16.11.2019–28.09.2020	259	252	Nortek Signature 100 (echosounder, ADCP, T, P)	**No**
M1-bio-2	79.589	28.088	22.02.2021–10.11.2021	259	245	Nortek Signature 100 (echosounder, ADCP, T, P)	**No**
M5-bio-1	77.082	35.036	11.08.2019–28.09.2020	147	136	Nortek Signature 100 (echosounder, ADCP, T, P)	**Yes**
M5-bio-2	77.082	35.058	12.10.2020–07.11.2021	144	140	Nortek Signature 100 (echosounder, ADCP, T, P)	**Yes**
AT800-bio-1	81.548	30.839	23.11.2019–29.09.2020	876	400	Nortek Signature 100 (echosounder, ADCP, T, P)	**Yes**
AT800-bio-2	81.548	30.839	30.09.2020–14.09.2021	872	453	Nortek Signature 100 (echosounder, ADCP, T, P)	**No**
Physics moorings							
M1-phy-1	79.593	28.094	05.10.2018–16.11.2019	259	20, 97, 155, 175, 218, 253	RBR Concerto (T,C,S,P)	-
M1-phy-2	79.583	28.073	16.11.2019–21.09.2020	252 20*, 98*, 155**, 175*, 215*	*RBR Concerto (T,C,S,P), **RBR Solo (T,P)	–	
M1-phy-3	79.583	28.059	20.02.2021–10.11.2021	252	20, 97, 180, 255	RBR Concerto (T,C,S,P)	–
M5-phy	77.08	35.04	13.10.2020–05.11.2021	148	126	Sea-Bird SeapHox2 (T,C,S,P,DO, pH)	–
AT800-phy-1	81.549	30.871	21.11.2019–22.09. 2020	867	13, 39, 45, 151,201,302, 408, 867	RBR Concerto (T,C,S,P)	–
AT800-phy-2	81.550	30.897	30.09.2020–20.11.2020	867	57, 103, 158, 307, 877	RBR Concerto (T,C,S,P)	

deployment are provided in Table 1. At *AT800* and at *M1*, different Signature100s were used during the first and second deployments. At *M5* the same instrument was redeployed after servicing.

2.3. Echosounder operation and data processing

The Signature100 echosounder operates in both wideband (68–113 kHz) and narrowband (70 and 120 kHz) modes. In this study we use only the narrow band data. No 120 kHz data were available for the *M5-bio-2* deployment due to a technical failure. The ADCP and echosounder pings are sequential and separated by a 1 s delay to allow time for two-way sound propagation and signal processing (Cutter et al., 2022; Velasco et al., 2018). Echosounder data were recorded at 20 s intervals using a bin size of 0.75 m. Binning of the data was done prior to any further processing or analysis. Target strength (TS; dB referenced to 1 m^2) and volume backscattering strength (S_v; dB referenced to 1 m^{-1}) were then obtained by converting the recorded squared amplitude values that result from internal processing of the raw data using the Nortek Ocean Contour software V.2.1.5. See Cutter et al., (2022) for further details. Echograms are presented as depth-timeseries of volume backscatter strength (S_v) (in dB re 1 m^{-1}, (Maclennan et al., 2002). S_v is the logarithmic version of the volume backscattering coefficient (s_V), which is proportional to the concentration of sound scattering organisms per unit volume.

Periods of rough weather, surface sea ice activity and occasionally marine traffic, introduced noise to the raw echosounder data. Noise was particularly a problem for data recorded at *AT800* due to the larger depth range, spanning the maximum range of the instrument. At depth ranges of more than 250 m, low signal to noise ratio typically meant that only schools with relatively high reflectance could be detected. Following the preliminary processing conducted within the Nortek Ocean Contour software V.2.1.5, additional spikes and background noise in the data were removed in two ways, firstly, all data points outside the range -110 dB re $m^{-1} \geq S_v \geq$ -20 dB re m^{-1} were removed. Secondly all data points where the instantaneous depth mean S_v was greater than 5 dB above the depth averaged 24-hour running mean were removed. Surface noise was removed separately by identifying any values of S_v within the uppermost bin (at approximately 2.5 m depth) which exceeded -65 dB and then tracking down through the water column removing all points until a bin with $Sv < -65$ dB was reached. While this method risks removing dense schools which are compressed against the surface, it proved effective in removing noise induced by surface processes.

The centre of mass of sound scattering layers (SL), also referred to as Weighted Mean Depth (WMD) was calculated following equation (1) (Gjøsæter et al., 2017).

$$WMD = \frac{\sum_{j=1}^{N} z_j s_{vj}(SL)}{\sum_{j=1}^{N} s_{vj}(SL)} \quad (1)$$

where z_j is the depth of depth bin j, s_{Vj} the volume backscattering coefficient for that depth interval, and N is the number of depth intervals. The area backscattering coefficient (s_a) was calculated from the volume backscattering coefficient (s_v), equations (2), which is related to the volume backscattering strength (S_v) by equation (3) (Maclennan et al., 2002).

$$s_a = \int_{z1}^{z2} s_v dz \quad (2)$$

$$S_v = 10 \bullet log10(s_v) \quad (3)$$

The echograms recorded at each mooring site are presented in their entirety to demonstrate how the density distribution of sound scattering organisms at each location changes over seasonal timescales. Timeseries of area backscattering coefficient are also presented in order to show how the depth integrated density of sound scattering organisms changes over time. As the details in the echograms cannot be resolved when looking at long-time records, we also present a series of five-day time-slices recorded during different seasons. Shorter time records reveal the often complex and organised vertical structure exhibited by the pelagic community and reveal details of the diel vertical migrations which are a common feature at each of the mooring sites. It should be noted however, that much of the detail in the echograms is lost even when looking at the five-day time-slices. Additionally, as the echograms do not include the lower 10 m–14 m of the water column, benthic associated organisms may remain undetected or may be detected only when they rise upwards during daily migrations.

2.4. Echosounder calibration

The Signature100s were not calibrated prior to deployment. Two of the instruments were calibrated after retrieval, these being the instrument deployed at *AT800-bio-1* and the instrument deployed at *M5-bio*. For these instruments we present calibrated data, for all other instruments the data are uncalibrated (Table 1). Therefore, an assessment of absolute abundance or interannual comparisons between moorings was not possible. Rather the data have value in allowing analysis of seasonal changes in abundance, and vertical distributions. An estimated gain of -50 dB has been subtracted from the uncalibrated S_v data to obtain values within a realistic range.

On-axis calibration was performed using a 25 mm diameter Wolfram tungsten carbide sphere, positioned at a range of approximately 5.5 m from the transducer. The calibration was performed during calm weather from a jetty near the IMR headquarters in Bergen, Norway, in a water depth of approximately 12 m. Calibration gain offset values for each echosounder and channel were then computed as 0.5 times the differences between the measured TS and theoretical TS of the standard sphere, following Cutter et al. (2022). Calibrated TS and S_v values were then obtained by adding the calibration gain to the uncalibrated values.

To distinguish 'fish-like' and 'zooplankton-like' scatters in the calibrated echograms we have followed the methods of Levine et al. (2023). These authors calculate the difference between 70 and 200 kHz volume backscatter. A classification of 'fish-like' scatters was applied where S_v was greater at 70 kHz, and a classification of 'zooplankton-like' scatters was applied where S_v was greater at 200 kHz. We apply the same technique here using 70 and 120 kHz volume backscatter, acknowledging that the narrower frequency range will create increased uncertainty. Possibly due to the narrower frequency range of our data it was necessary to set an upper limit on the volume backscatter for a 'fish-like' classification. Hence, all data where $Sv_{70\ kHz} \leq Sv_{120\ kHz}$ were classified as 'zooplankton-like' scatters and all data where $Sv_{70\ kHz} \geq Sv_{120\ kHz}$ and $Sv_{70\ kHz} \geq -70$ dB ref 1 m^{-1} were classified as 'fish-like' scatters. Fig. 2 shows an example echogram of 70 kHz volume backscatter recorded at *M5-bio-1*, along with the corresponding difference plot ($S_{v\ 70\ kHz}$–$S_{v\ 120\ kHz}$) calculated as described above. This method is applied to data from the *M5-bio-1* and *AT800-bio-1* moorings for which calibrated 70 kHz and 120 KHz data are available.

2.5. Acoustic doppler current profiler operation and data processing

The Signature100 ADCPs operate at a centre frequency of 100 kHz and were configured to sample at an interval of 2700 s over an averaging period of 180 s, and a depth bin size of 5 m. Orientation data were recorded by the internal altitude and heading reference sensors, which measure magnetic compass heading and tilt (Velasco et al., 2018). Compass heading values were adjusted by the magnetic declination for the study area, based on the World Magnetic Model of 2020. Processing of the ADCP data was performed using the Nortek Ocean Contour Software V.2.1 5. ADCP data with mean correlations over all beams of less than 50 % were removed as were data with a 'percent good' value of less than 50 %, where the percent good is a measure of data quality and

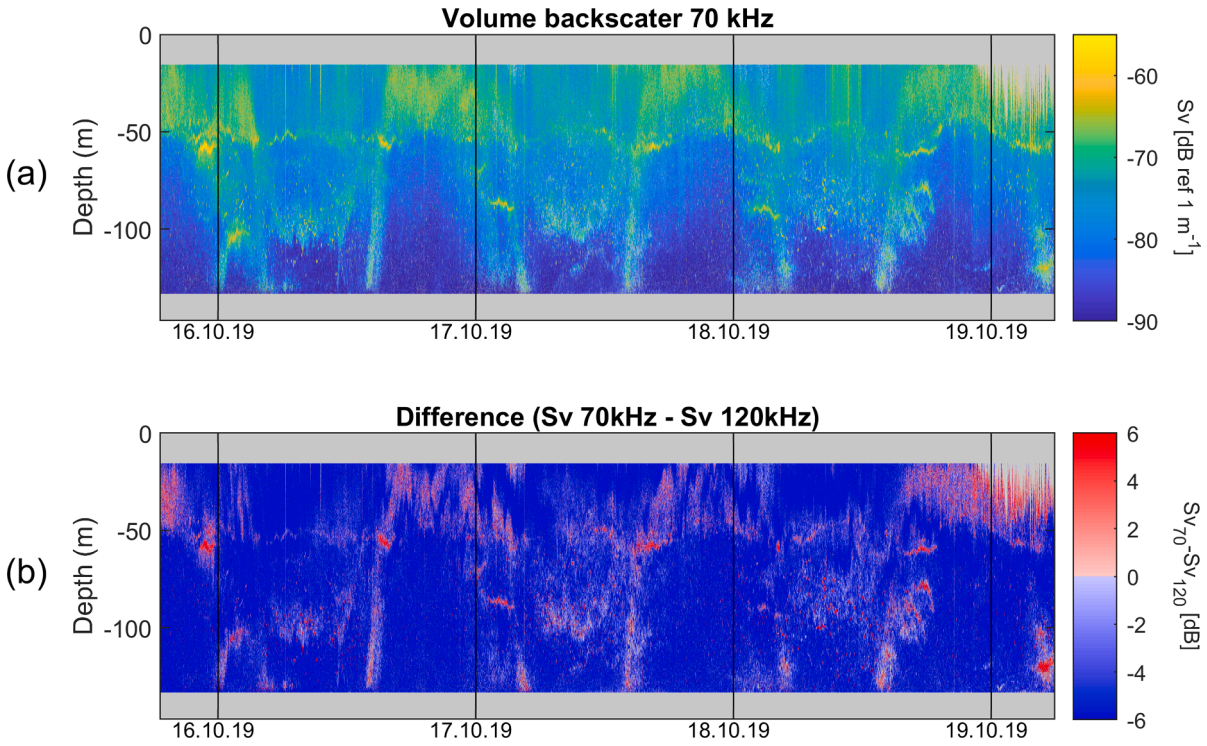

Fig. 2. (a) A short example echogram showing 70 kHz volume backscatter recorded during mid-October at M5 and (b) difference in volume backscatter (S_v at 70 kHz minus S_v at 120 kHz) indicating the distribution of fish-like scatters in red (S_v 70 kHz $\geq$ S_v 120 kHz and S_v 70 kHz ≥ -70 dB ref 1 m^{-1}) and zooplankton-like scatters in blue (S_v 120 kHz $\geq$ S_v 70 kHz).

defines the ratio of good pings per total pings for each ensemble profile. Tides calculated using the Arctic TOPEX tidal model (Egbert and Erofeeva, 2002) were subtracted from the ADCP data.

2.6. Moorings with physical and chemical sensors

Each acoustic mooring was located close to a second mooring recording physical and chemical data. *M1-Bio* was located close to the *M1* physics mooring described in detail by Lundesgaard et al. (2022) at which temperature and salinity data were collected at several depths throughout the water column every 1 to 5 min (Table 1). The *AT800-bio* moorings were located close to the *AT800* physics mooring, part of the A-TWAIN mooring array (Renner et al., 2018). The *AT800* physics mooring was located at a water depth of approximately 880 m, within the core of the Atlantic Water Boundary current. Temperature and salinity data were recorded at several depth levels every 5 min (Table 1; Lundesgaard et al., 2022). At *M5,* temperature, salinity, pressure, and oxygen were recorded at 126 m depth by a Sea-Bird SeapHox2 throughout the duration of the *M5-Bio-2* deployment. Temperature and salinity data recorded at *M1* and *AT800* were interpolated onto a 10 m resolution vertical grid and the pycnocline depth was estimated from the gridded data. It should be noted that due to the relatively coarse resolution of the temperature and salinity sensors physical gradients can only be approximated. The estimated depth of the 34.7 g kg^{-1} isohaline was chosen to approximate the boundary between the more saline Atlantic influenced water at depth and the overlying Polar Water.

2.7. Supporting data

Gridded daily mean time series of Sea Surface Temperature (SST), Sea Ice Concentration (SIC) and surface winds at 0.05-degree resolution were obtained from the E.U. Copernicus Marine Service Information website. SST and SIC were extracted from the product: Global SST & Sea Ice Analysis, L4 OSTIA, 0.05° daily; https://doi.org/10.48670/moi-00165. Surface winds were extracted from the product: Global Ocean Wind L4 Near real Time 6 hourly Observations https://doi.org/10.48670/moi-00184. Timeseries were extracted from the gridded products at the nearest available grid points to the mooring locations. Day lengths and timings of sunrise and sunset were calculated using the NOAA Solar Calculator available at https://gml.noaa.gov/grad/solcalc/calcdetails.html.

3. Results

In this section we describe data collected at each mooring site in turn, starting with the most southerly site and progressing northwards. The temporal evolution in currents, water column hydrography and SIC are described as these are fundamental to the following interpretation of the echograms. We continue by describing how the density and depth distribution of macrozooplankton and fish varied over time at each mooring location.

3.1. Physical environment and acoustic backscatter at M5

Sea ice was present at *M5* in variable concentration from December 2019 to June 2020 (Fig. 3a). There was considerably less sea ice present during the winter of 2020–21, with low concentrations of sea ice during parts of January, February and March, and only occasional inflows of sea ice during May and June. Sea surface temperatures (SST) at *M5* reached maximum values towards the end of August of 5.8 °C in 2020 and 4 °C in 2021 (Fig. 3b). During autumn SSTs cooled rapidly and remained sub-zero from early November through to early July of the following year. The near-bottom water temperature at *M5* remained close to or below zero throughout the year, with maximum near bottom water temperatures in late winter, prior to the break-down of the stratification. During both years, complete vertical mixing of the water column during the late winter or early spring followed the disappearance of the sea ice. In 2020 this occurred during a temporary break in the sea ice in early February, while during 2021 the seasonal disappearance of the sea-ice in mid-March resulted in a later break-down of the stratification. During

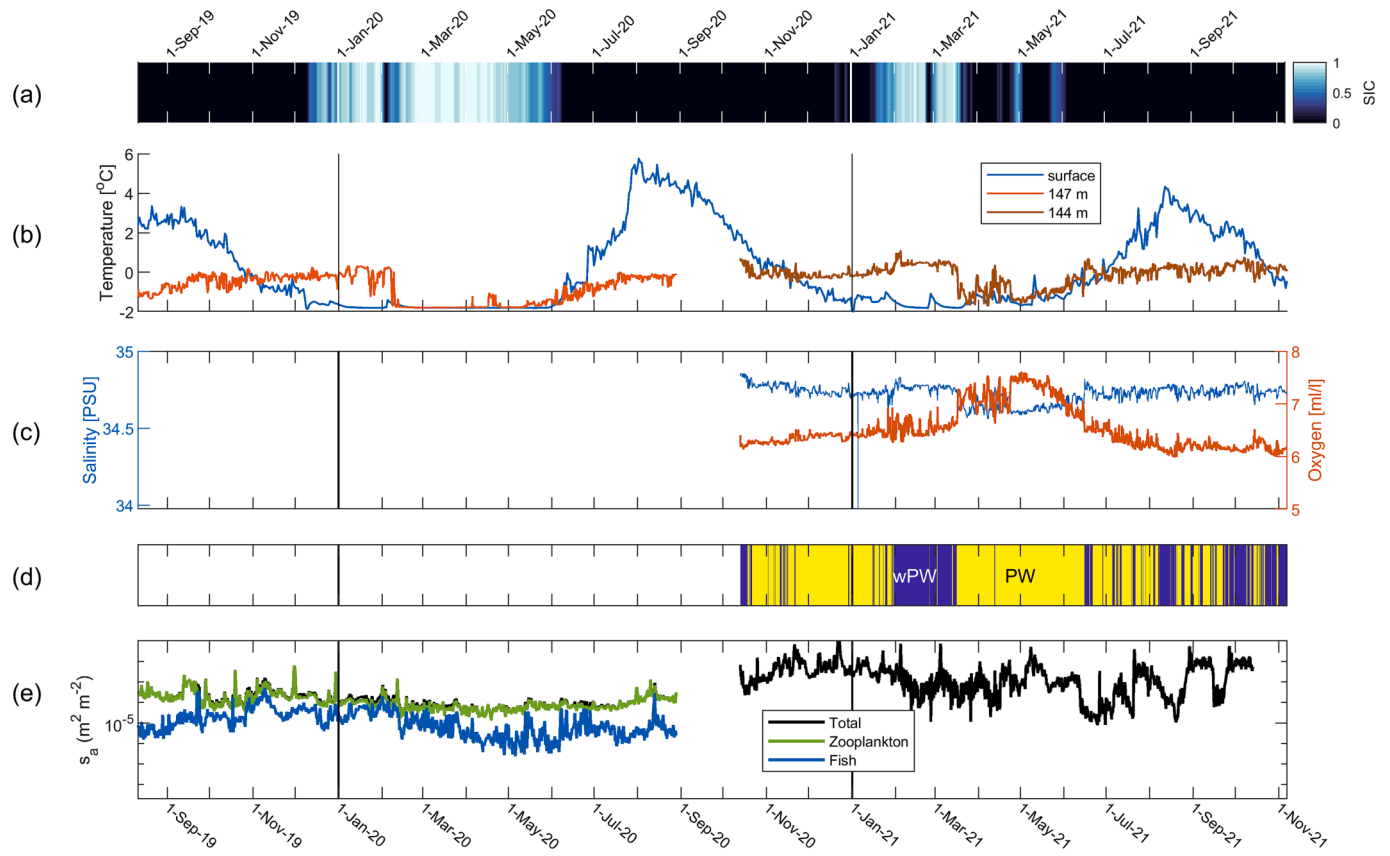

Fig. 3. Time series at *M5-bio* of (a) sea ice concentration, (b) SST and temperature at 146 m, (c) oxygen and salinity at 144 m depth, (d) water mass characterisation at 144 m depth, with Polar Water (PW) in blue and Warm Polar Water (wPW) in yellow, and (e) area backscattering coefficient of fish like scatters (blue) and macrozooplankton like scatters (green) and the total area backscattering coefficient (black). Note the logarithmic scale in Figure (e).

spring 2020, vertical mixing of the water column in early February was followed by the return of the sea ice for another 3.5 months during which period the water column maintained a uniform temperature of −1.7 °C (Fig. 3a and 3b). Vertical mixing was indicated by a rapid decrease in the bottom temperature (Fig. 3b) and salinity (Fig. 3c), as well as a rapid increase in near bottom dissolved oxygen concentration (Fig. 3c) and a change in the near bottom water mass composition from wPW to PW (Fig. 3d). Throughout April, May and June, surface and near bottom temperatures and bottom salinity gradually increased, while dissolved oxygen steadily decreased, likely due to consumption during remineralisation. Stratification was re-established via warming of the surface layer in early July 2021, at about the same time as in 2020, despite a much earlier retreat of the sea ice. Notably, the bottom water temperature was on average 0.7 °C warmer during 2021 as compared to 2020.

The detided depth mean velocity at *M5* was predominantly towards the east or northeast at all depths, although there was a clockwise rotation in current direction with increasing depth, most pronounced during the summer months (progressive vector diagrams are included as supplementary material S1). Strong pulses of NE flow (0.2–0.6 m s^{-1}) were observed intermittently throughout the timeseries and were typically associated with a change in water mass characteristics. Comparison to satellite wind data (not shown) revealed no association of such events with significant wind events, suggesting they may have resulted from passing eddies.

The area backscatter coefficient which represents the depth integrated density of macrozooplankton, and fish present (Fig. 3e) is presented separately for 'fish-like' scatters and 'zooplankton-like' scatters for the 2019–20 period. (Note that zooplankton detected within the 70–120 kHz frequency range are macroplankton in addition to some larger mesoplankton.) It was not possible to distinguish fish-like and zooplankton-like scatters for the 2020–21 period due to the lack of 120 kHz data. There was a marked contrast between the total density of organisms present during the winters of 2019–20 and 2020–21. Seasonal peaks in total volume backscatter occurred during autumn and during mid-winter of both 2019 and 2020, however, the winter (DJF) mean area backscattering coefficient during 2020–21 was 3.3 time higher than during 2019–20. Following vertical mixing of the water column in early February 2020, when the water column had a uniform temperature of −1.7 °C, the density of macrozooplankton and fish present was relatively low. After the onset of thermal stratification in July 2020, the concentration of sound scattering organisms increased. By comparison, during 2021, an absence of sea ice allowed the water column to gradually warm and there was a relatively high density of macrozooplankton and fish present at *M5* throughout May and during much of June and July 2021.

Some similarities in the seasonal evolution of the vertical distribution of scatterers during 2019–20 and 2020–21 can be identified in the echograms of 70 kHz volume backscatter (Fig. 4b). During both 2019 and 2020 a strong echo located between 30 m and 40 m depth developed in the late summer. This echo gradually deepened throughout the winter months, resembling the development and deepening of the surface PW layer, and intersected the bottom at about the same time as the surface and bottom temperature records begin to overlap (indicating complete vertical mixing; Fig. 3b). This echo exhibited a frequency response characteristic of a density interface and most likely represented the development and deepening of the pycnocline. During the winter of 2019–20 the water column below the pycnocline was relatively empty of sound scattering organisms. By comparison during the winter of 2020–21 the water column under the pycnocline contained a particularly high density of organisms. The pycnocline echo is difficult to see when looking at the entire echograms but its location during 2020 is

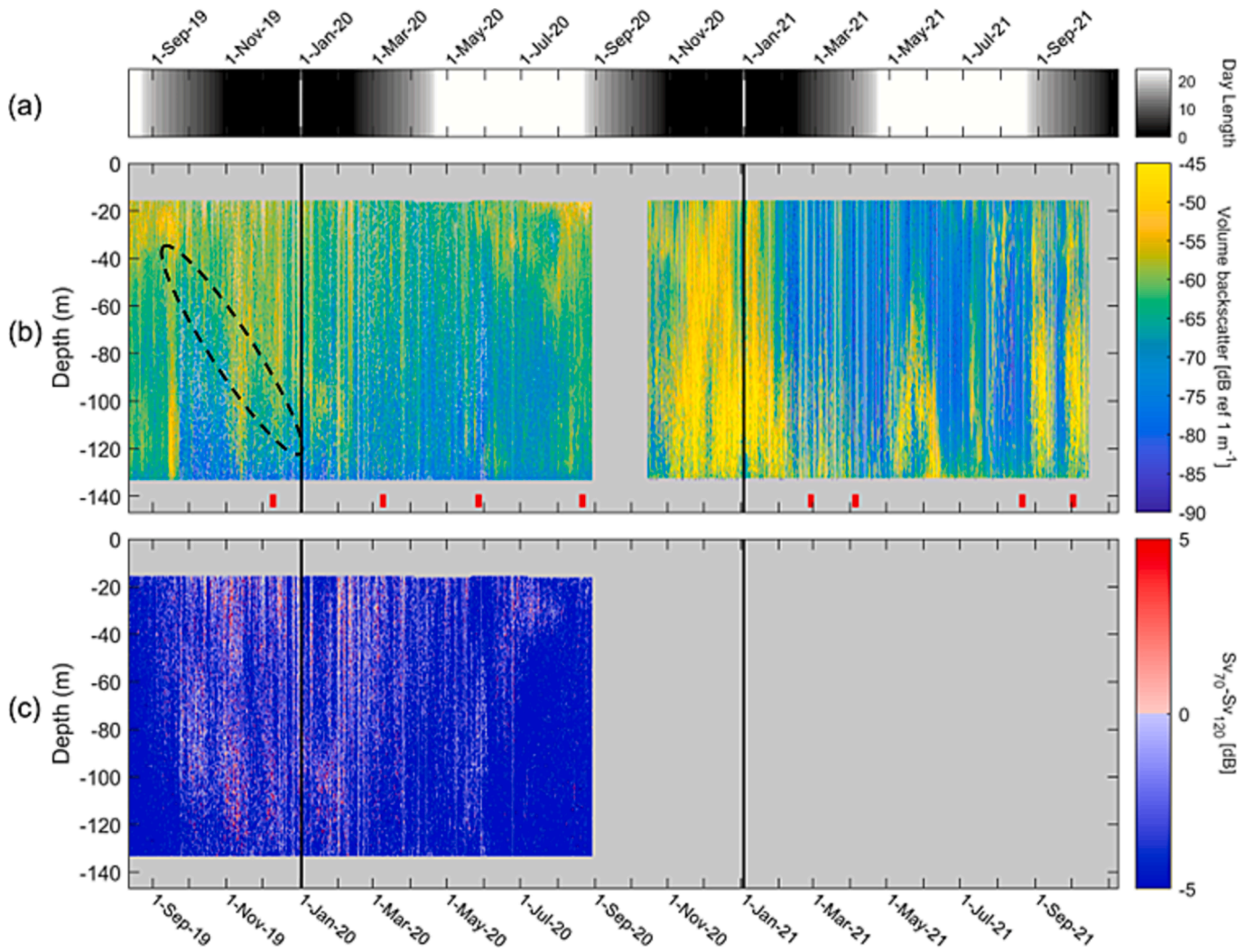

Fig. 4. Timeseries at *M5* of (a) number of hours the sun is above the horizon each day, (b) echogram of 70 kHz volume backscatter (S_v) and (c) difference in volume backscatter (S_v at 70 kHz minus S_v at 120 kHz), where red indicates bins where S_v is greater at 70 kHz (fish-like scatterers), and blue indicates bins where S_V is greater at 120 kHz (zooplankton-like scatterers). The grey dashed line in figure b circles the location of the deepening density interface during winter/spring 2020. The red marks at the bottom of figure b indicate the periods shown in the five-day duration echograms of 70 kHz volume backscatter presented in Fig. 5.

circled by a dashed line in Fig. 4b. The pycnocline depth can been seen more clearly in the 5-day duration echograms shown in Fig. 5 (in Fig. 5a the pycnocline is at about 40 m depth and in Fig. 5b at about 80 m depth.) It is evident from Fig. 5 that the pycnocline depth influenced the vertical distribution of sound scattering organisms over diurnal to seasonal timescales.

The difference between 120 kHz and 70 KHz volume backscatter (Fig. 4c), reveals the vertical distribution of fish within the water column. Fish-like scatterers were distributed throughout the water column during autumn 2019, before becoming increasingly concentrated below about 100 m depth during the first half of the winter. Following vertical mixing of the water column the total density of fish declined (Fig. 3e). During March and April 2020, when the water column remained vertically mixed, fish were observed mostly within the upper 60–80 m of the water column. During May fish were distributed throughout the water column, concentrated at increasingly deeper depths as the month progressed. Following the onset of vertical stratification due to surface warming in late June and July, the total density of fish present increased (compare Fig. 3b and 3e). During the late summer fish were concentrated in the upper 40 m of the water column (Fig. 4c).

Superimposed on the seasonal variability was significant variability occurring over timescales of days to weeks which typically coincided with changes in vertical stratification and bottom temperature. A particularly pronounced example of this occurred in mid-September 2019 (see Fig. 5a), coinciding with a small increase in near-bottom temperature (Fig. 3c). Prior to this event, between 12th August and 12th September 2019, a relatively high density of macrozooplankton were distributed throughout the water column (Fig. 3e and 4b). As was commonly observed at *M5-bio,* three distinct sound scattering layers were present at this time, each performing synchronous but differing DVMs (Fig. 5a). One sound scattering layer, performing an inverse migration, rose upwards during the day, and descended at night (see the first 3 days in Fig. 5a where this layer is labelled [1]). A second sound scattering layer located near the bottom during the day migrated up into the water mass above the pycnocline during the night (nocturnal migration) this layer is labelled [2] in Fig. 5a. Additionally there was a deepening of organisms residing in the surface layer during the day and an ascent towards the surface around dusk (this is seen most clearly during the last two days included in Fig. 5a (22nd and 23rd September) and is labelled [3]. On 22nd September there was a sudden and rapid decline in the density of macrozooplankton present, after which the sound scattering layer performing the inverse migration disappeared completely, while the other two layers remained, but at lower densities. These events demonstrate how rapidly the density and community

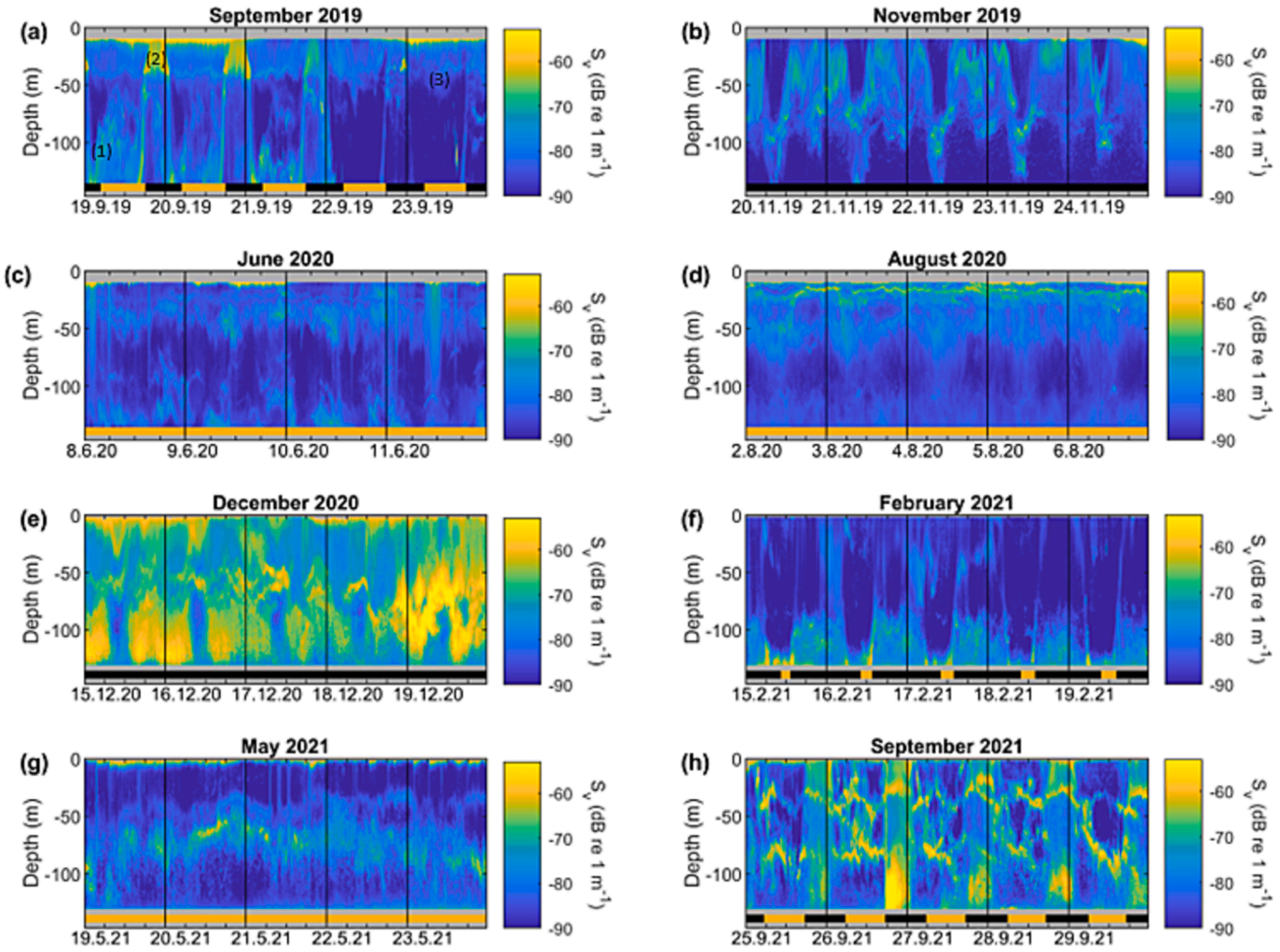

Fig. 5. A series of five-day duration echograms of 70 kHz volume backscatter during different seasons extracted from the *M5-bio* echograms, in (a-d) data are from the *M5-bio-1* mooring and in (e-f) data are from the *M5-bio-2* mooring. The duration the sun is above the horizon (yellow bars) and below the horizon (black bars) is indicated at the bottom of each figure panel.

structure of macrozooplankton can change in response to physical forcing.

DVM's were observed at *M5* during all seasons except mid-summer, with many different types of DVM observed (Fig. 5). Fig. 5e shows an example of reverse DVM, with an ascension of organisms into the upper water mass around mid-day. This occurred under the ice during the polar night (mid-December) at a time when the density of macrozooplankton present was particularly high. The acoustic data collected at M5 thus reveal the persistent presence of a macrozooplankton community on the great Bank, performing DVMs throughout the winter months. At other times of the year, particularly during the late summer and autumn, multiple thin scattering layers could be discerned at different depths. Where multiple scattering layers existed, each performed synchronous but different DVMs, forming complex vertical structures (e.g., Fig. 5d and 5h).

3.2. Physical environment and acoustic backscatter at M1

Fractured sea ice was present when both the *M1-bio-1* and *M1-bio-2* moorings were deployed (during November 2019 and February 2021) and persisted until early July 2020 and until early August 2021 (Fig. 6a). The water column structure at *M1* was characterised by cool and fresh PW overlaying warmer and more saline Atlantic influenced wPW (Fig. 6b-d). The surface PW layer exhibited seasonal variability characterised by increasing salinity due to brine rejection throughout the winter months, followed by freshening and warming after the ice began to melt in June. The underlying wPW layer was typically warmer and more saline during the winter months, and relatively fresh and cool during the summer. The thickness, temperature and salinity characteristics of this layer were, however, highly variable, particularly during 2020. The wPW layer was at its thickest and warmest during the winter of 2019/2020. A sudden change in conditions on 28th February 2020 then resulted in complete disappearance of the wPW layer, with PW briefly filling the entire water column. Similar events also occurred during late March and early April with a reduced volume of wPW throughout May, June and July 2020. By comparison, wPW occupied the lower water column throughout 2021.

Currents at *M1-bio* were strongly constrained by bathymetry and primarily orientated in the along-slope direction (38° clockwise relative to true north) at all depths (Fig. 6e). The net annual transport was towards the SW, which corresponds to a transport of off-shelf waters into the Kvitøya Trough from the north. During the late spring and early summer, however, a weak but persistent reversal in current direction was observed, such that the net transport was towards the mouth of the Kvitøya Trough over a period of several months. Progressive vector plots showing velocities at M1 are included as supplementary material S2.

We note a relationship between SIC and current direction, although the relationship varied seasonally. South-westerly flow dominated in the absence of sea ice and under low sea ice concentration conditions (when the sea ice concentration was below 20 %, residual (time-averaged)

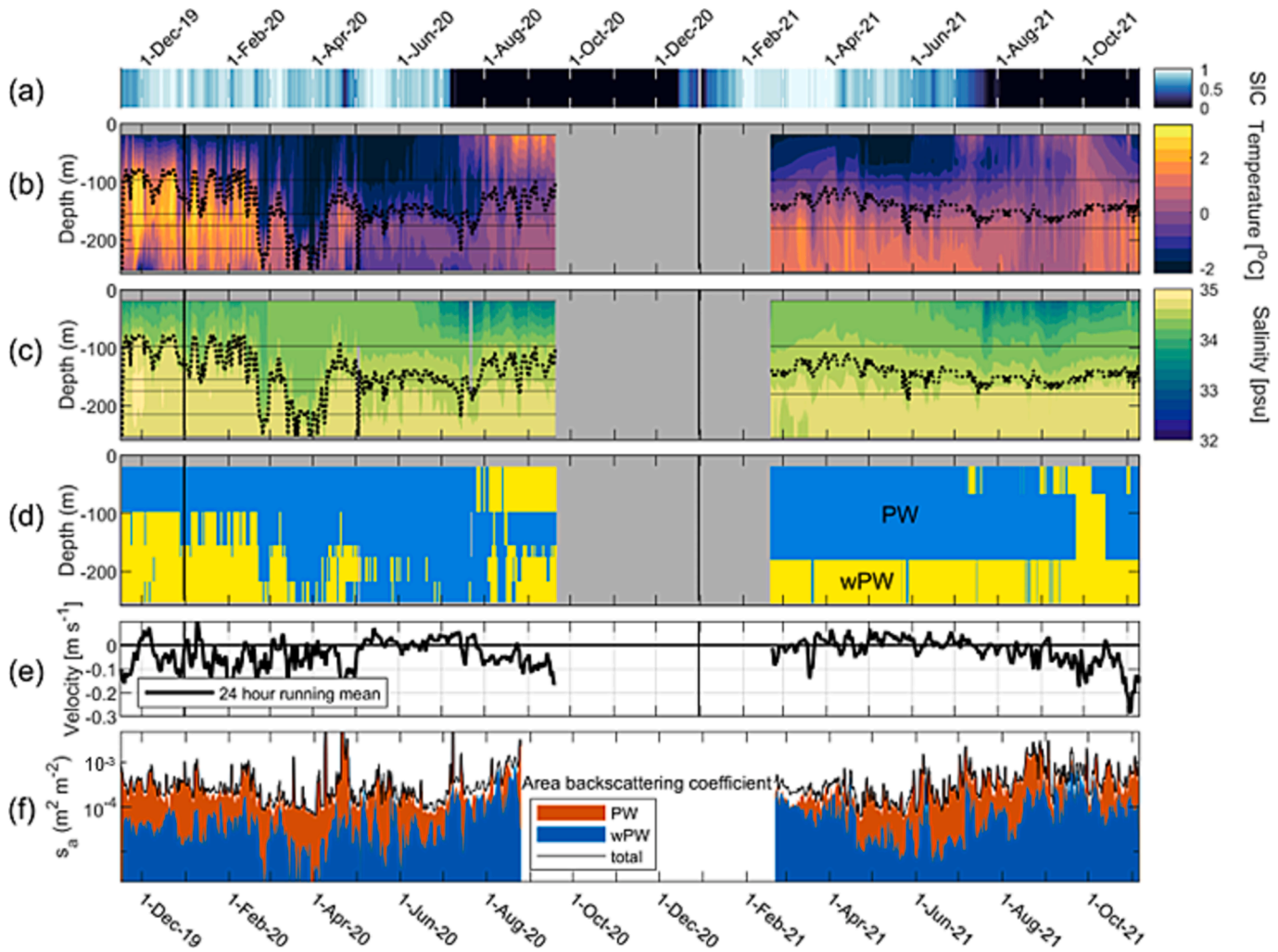

Fig. 6. Time series at *M1* of (a) sea ice concentration, (b) depth-time series of temperature, (c) depth-time series of salinity, (d) water mass distribution and (e) along channel depth mean velocity (positive values indicated transport into the Kvitøya Trough from the north) and in (f) area backscattering coefficient within PW (blue), wPW (red) and the total area backscattering coefficient (black). The dashed lines in (b and c) represents the estimated depth of the 34.7 isohaline, used here to define the boundary between the more saline Atlantic influenced water at depth and the overlying Polar Water.

currents were towards the southwest 79 % of the time). Conversely there was an increased tendency for currents towards the northeast in the presence of sea ice, particularly during spring when the current reversed as soon as the sea ice disappeared. During winter, currents were stronger and exhibited greater variability over synoptic timescales. Over the period December to April a significant positive correlation existed between SIC and depth mean along-slope current speed ($r = 0.55$; $P = 0.00$). Just as a relationship was noted above between the SIC and the prevailing current direction, we also note a relationship between the current direction and the water column structure, consistent with the findings of Lundesgaard et al. (2022). This can be summarised as an increase in the temperature, salinity, and volume of the lower water mass during periods of SW currents and low SIC or ice-free conditions. Hence, northerly flow through the Kvitøya Trough brings Atlantic influenced water originating from the AWBC into the northern Barents Sea.

As the echosounder data at *M1* are uncalibrated, absolute values remain unknown and it is not possible to distinguish fish and macroplankton at this site. However, these data provide information on how the vertical distribution and density of organisms changed relatively over time and give valuable insight into the temporal processes occurring. Time series of area backscattering coefficient (Fig. 6f) show that the density of sound scattering organisms at *M1-bio* was maximum during then late-summer/early-autumn. The disappearance of the sea ice in July (Fig. 6a) was marked by a rapid increase in the density of sound scattering organisms, with the highest concentration of organisms recorded between July and September of both years. High concentrations of organisms were also present throughout the winter, suggesting, as on the Great Bank, the presence of a macrozooplankton community in the northern Barents Sea throughout the winter period. The lowest density of sound scattering organisms at M1 occurred during the spring and early summer.

Day length at *M1-bio* is shown in Fig. 7a, alongside echograms of 70 kHz volume backscatter in Fig. 7b. The echograms exhibit distinct seasonal variability in both the concentration and vertical distribution of sound scattering organisms, although there are also some considerable differences between the two study years. From the beginning of the record in November 2019 until mid-February 2020 sound scattering organisms were primarily located within the upper PW layer. At this time there was a persistent sound scattering layer situated within the upper portion of the pycnocline between approximately 80 m and 150 m depth (Figs. 7b and 8a) and schools of macrozooplankton or fish were distributed throughout the upper PW layer. Although fish cannot be distinguished in the uncalibrated data, the dense schools present near the surface under the ice during winter (see the 5-day time slice presented in Fig. 8a) have the appearance of fish schools. Below the

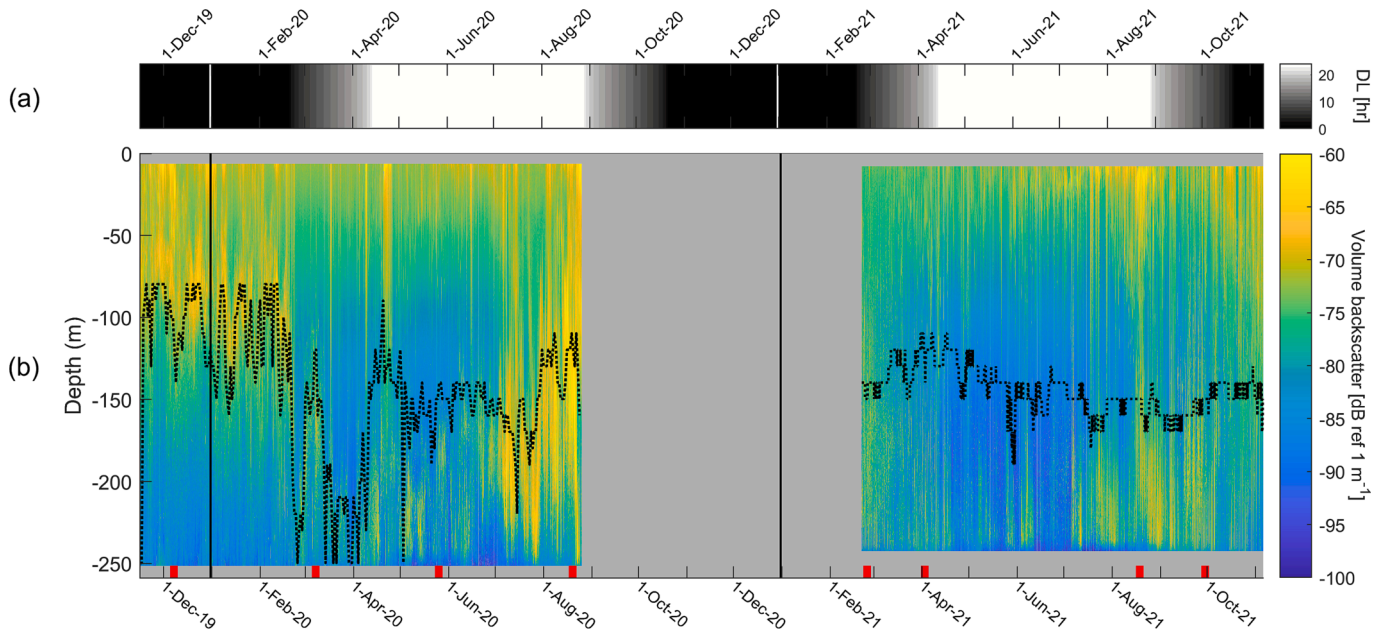

Fig. 7. Timeseries at *M1* of (a) number of hours the sun is above the horizon each day and (b) echogram of 70 kHz volume backscatter (S_v). The dashed line in (b) represents the estimated depth of the 34.7 isohaline, used here to define the boundary between the more saline Atlantic influenced water at depth and the overlying Polar Water. The red marks at the bottom of figure b indicate the periods shown in the five-day duration echograms of 70 kHz volume backscatter presented in Fig. 8.

pycnocline, during winter, sound scattering organisms were distributed diffusely rather than forming schools or layers, and the density of organisms decreased with increasing depth. After 5th February organisms residing within the pycnocline began to migrate downwards during the day, establishing a full depth DVM over the course of about 5 days. There was a sudden decline in the concentration of organisms throughout the entire water column on 24th February 2020, which coincided with a reversal in current direction and the temporary disappearance of the underlying wPW layer. On this and several subsequent occasions when PW filled the water column, the lower scattering layer which remained confined to the deep wPW layer (Fig. 8b), completely disappeared. Following the reappearance of the deep wPW layer on 1st March 2020, through early July, two distinct sound scattering layers were present, one below the pycnocline and a second within the upper 100 m, (Fig. 8c). During this period the intermediate water column contained very few sound scattering organisms. Similarly, from late February 2021 through until early August 2021, two distinct sound scattering layers were observed near the bottom and near the surface, with very few organisms present between about 100 m and 200 m depth. The relatively low concentration of sound scattering organisms during the late spring and early summer of 2021 as compared to 2020 may reflect the longer duration over which the current direction was reversed during 2021. During spring and early summer, the density distribution within both the near-surface and near-bottom scattering layers was patchy and DVMs of less than 50 m vertical extent were observed within both layers. The upper and lower scattering layers remained mostly within their respective water masses, exhibiting little evidence of interaction between the layers.

When the ice concentration was low (less than 0.4) such that the water column was influenced by wind forcing, a negative correlation ($r = -0.49$, $P = 0.00$) existed between the depth mean along channel velocity (positive out of the channel) and the near bottom water temperature, with warmer near bottom temperatures associated with an increased volume of wPW present at the mooring site. Typically, the area backscattering coefficient was higher when both PW and wPW were present. A negative correlation ($r^2 = -0.47$, $P = 0.00$) existed between the depth mean along-channel velocity and the area backscattering coefficient, and between the bottom temperature and the area backscattering coefficient ($r^2 = -0.65$, $P = 0.00$) at M1, indicating a higher density of organisms present when there was a greater inflow of wPW. Correlation plots are included as supplementary material S3.

When the ice disappeared early in July, there was a rapid increase in the density of sound scattering organisms (compare Figs. 6a and 7b), likely indicative of a post-melt proliferation in macrozooplankton following a phytoplankton bloom. This increase in macrozooplankton density occurred more rapidly and was more pronounced during 2020 when the ice persisted until early July. During July and August 2020, the zooplankton were concentrated in the region of the pycnocline (Fig. 7b; Fig. 8d). During 2021 when the SIC throughout spring was considerably less than the previous year, the late summer proliferation of zooplankton was more modest but longer in duration. The vertical distribution of organisms during late summer 2021 differed considerably from the previous year, with organisms concentrated in two distinct layers, deep layer within the wPW and a second within the upper 100 m (Fig. 7 and compare Fig. 8d and 8h). In late July, organisms residing in the deep wPW layer began performing DVMs across the pycnocline, entering the upper layer for a few hours around midnight. During August, warming of the upper 50 m coincided with an increase in the concentration of sound scattering organisms in the upper water column, and the establishment of up to three distinct sound scattering layers. After the onset of 24-hour darkness in early October 2021, there was an upward migration of sound scattering organisms, an increase in the concentration of organisms in the upper 150 m of the water column and a decrease in the concentrations of organisms below 150 m depth. The vertical distribution of organisms thus began to look similar to that observed during the previous winter (2019–20).

3.3. Physical environment and acoustic backscatter at AT800

Sea ice was present at *AT800* from mid-winter through until the late summer of both 2020 and 2021 (Fig. 9a). Temperature and salinity records indicated the presence of a relatively fresh and cool PW layer at the surface throughout the year (Fig. 9b and 9c). The temperature of this fresh surface layer remained sub-zero under the ice, warming after the ice disappeared in late summer to reach a maximum value of 3.7 °C in August 2020. A pycnocline at approximately 120 m depth separated the

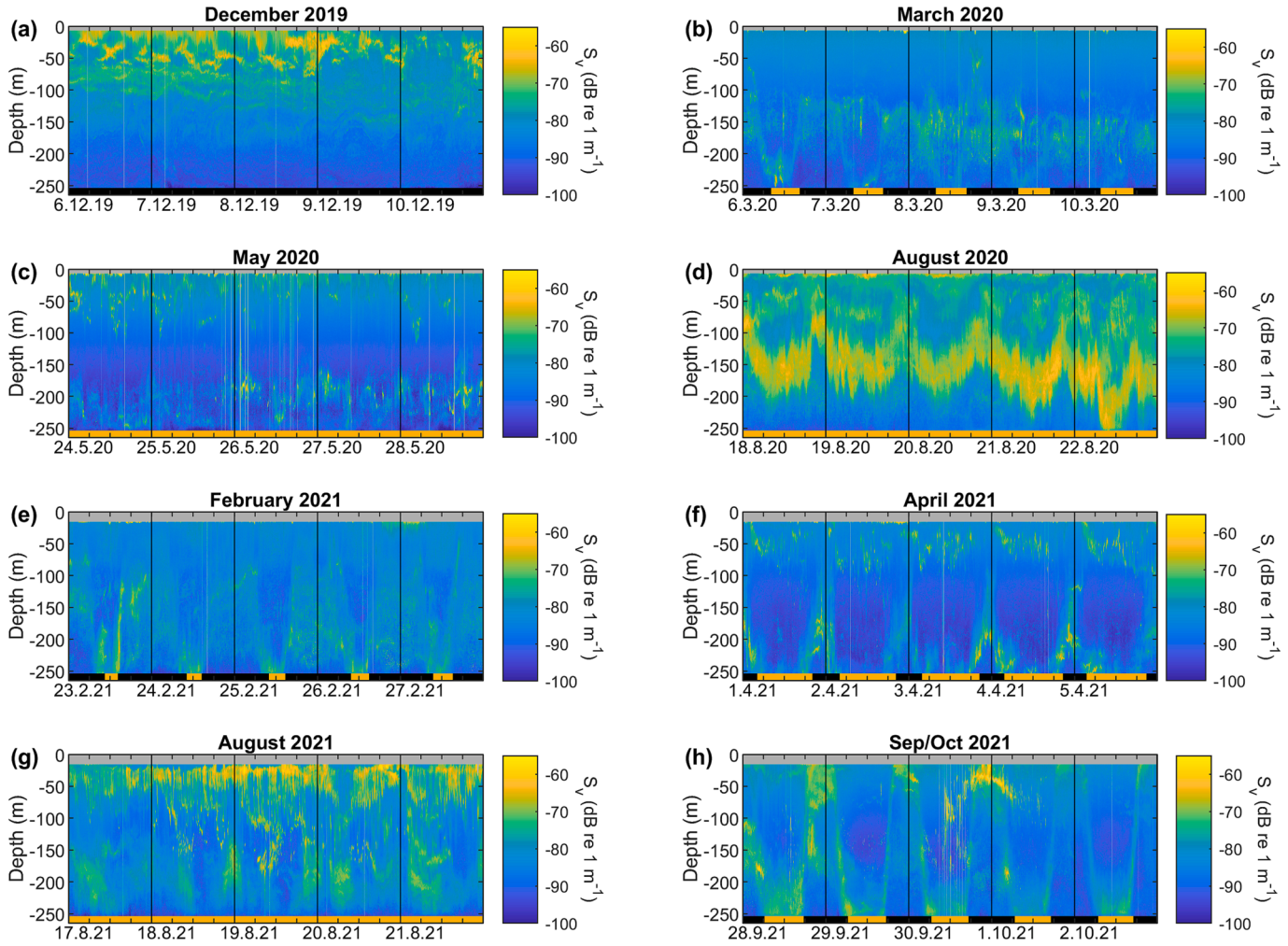

Fig. 8. A comparison of five-day duration echograms of 70 kHz volume backscatter during different seasons, extracted from the *M1-bio* echograms, in (a-d) data are from the *M1-bio-1* mooring and in (e-f) data are from the *M1-bio-2* mooring. The duration the sun is above the horizon (yellow bars) and below the horizon (black bars) is indicated at the bottom of each figure panel.

fresh surface layer from the more saline and typically warmer modified Atlantic water below. The depth range of the warm intermediate layer was difficult to define due to the coarse vertical spacing of the temperature and salinity sensors, but it was typically located between approximately 100 m and 500 m depth. The *AT800* moorings were located on the continental slope in a location characterised by strong and persistent along-slope eastward velocities (Fig. 9d). Stronger and more persistent currents were recorded during the second (*AT800-bio-2)* deployment. The strength of the shelf edge current varied seasonally, with the strongest depth mean transport observed during winter (2019–20: 0.17 m s^{-1}; 2020–21: 0.27 m s^{-1}) and the weakest during summer (2020: 0.08 m s^{-1}; 2021: 0.13 m s^{-1}). There was also considerable sub-seasonal scale variability in the strength of the current and occasional short-lived reversals in current direction. The most significant reversal in current direction occurred towards the end of February 2020 when weak westward velocities persisted over several days (Fig. 9d). The temperature of the warm intermediate layer was highest in late January when it reached 3.4 °C in 2020 and 4.7 °C in 2021, reflecting the stronger AWBC recorded during winter 2020–21 as compared to the previous year. The warm intermediate layer cooled throughout the spring and early summer, reaching a minimum of 0.85 °C in early July 2019 and of 1.1 °C in mid-May 2020, again reflecting the seasonality in the AWBC.

The area backscattering coefficient (Fig. 9e) has been calculated separately for fish-like and zooplankton-like scatterers for the first deployment at *AT800*. This was not possible for data collected during the second deployment at *AT800* as the echosounder data from this period was uncalibrated. It should also be noted that due to the deeper depth of the echosounder during the second deployment and the slightly different physical environment (with a stronger shelf edge current), the two timeseries of area backscattering coefficient presented in Fig. 9e are not directly comparable. Finally, it is evident that range of the echosounders was not sufficient to collect good data throughout the water column, with only particularly intense schools or layers detected beyond a range of approximately 200 m–250 m. We therefore interpret the *AT800* acoustic data with caution.

The density of macrozooplankton-like scatterers present at *AT800* was relatively low throughout winter and minimum during February (Fig. 9e). The macrozooplankton density increased slightly during spring and then decreased again in early summer before reaching maximum values following ice melt in August. High macrozooplankton densities then persisted throughout the early autumn (Fig. 9e). Conversely, the density of fish-like scatterers present increased throughout the winter, with the highest monthly mean during February. Throughout spring the density of fish-like scatterers declined, and fish were almost absent during June. During the late summer and early autumn the density of fish-like scatterers present increased gradually, with short-lived peaks during August and high densities of fish present during October.

The *AT800-bio-1* echogram (Fig. 10b) reveals the existence of a thick

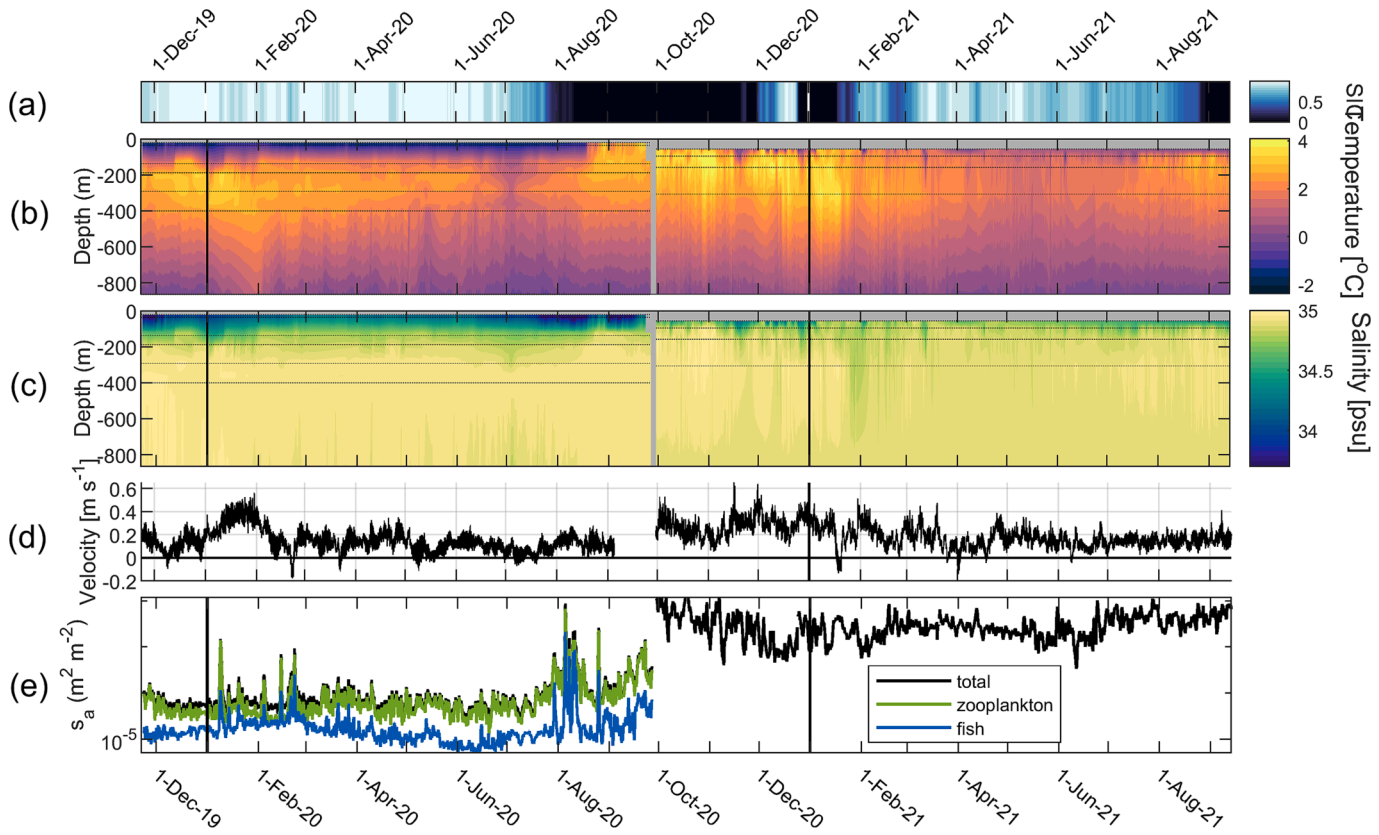

Fig. 9. Time series at *AT800* of (a) sea ice concentration, and (b) depth-time series of water temperature, (c) salinity, (d) depth-mean along slope velocity (positive indicates an approximately eastward direction) and (e) area backscattering coefficient of fish like scatters (blue) and macrozooplankton like scatters (green) and the total area backscattering coefficient (black).

mesopelagic sound scattering layer, present throughout most of the year except for mid-winter. This mesopelagic sound scattering layer was located within the AWBC, with its upper boundary proximal to the halocline. Fish were commonly situated within the lower region of the mesopelagic sound scattering layer, deeper in the water column than the macrozooplankton. Fewer sound scattering organisms were detected in the overlying polar water layer, however, thin and dense schools or layers of macroplankton were present in the upper 100 m throughout much of the year (as seen in Fig. 11a, 11b and 11c). During mid-winter sound scattering organisms were distributed more diffusely throughout the upper part of the water column and no distinct sound scattering layer could be discerned. During December the WMD (calculated over the entire depth range of the measurements) was situated at less than 100 m depth. From early February 2020 a distinct mesopelagic sound scattering layer became established, which spanned a depth range of almost 200 m (Fig. 10b and Fig. 11). Throughout spring the WMD began to deepen, reaching close to 300 m depth by early April 2020, and then remaining between 200 m and 300 m depth until late June 2020. At the end of June 2020, the centre of mass of the sound scattering layer ascended upwards to ~200 m depth, while the upper boundary of the sound scattering layer, now in the epipelagic, fluctuated between 90 m and 198 m (Fig. 11d). This ascension of the mesopelagic sound scattering layer, which persisted throughout most of July, coincided with both a reduction in SIF and a sharp reduction in the strength of the slope-current (and the Atlantic Water inflow). Throughout late August and September, the echogram data were very noisy with many gaps. However, it is evident that the deep scattering layer descended at the beginning of August. During the late summer 2020 the thickness and density of the mesopelagic sound scattering layer reached a seasonal maximum. At this time the scattering layer was more than 300 m thick.

DVMs of organisms within the mesopelagic sound scattering layer were observed at *AT800* during spring and autumn. During spring DVM began on 1st March (the day of the first sunrise) and continued until early May (as seen in Fig. 11b and 11f). The onset of DVM began with organisms descending downwards during the day, followed by a gradual deepening of the centre of mass of the sound scattering layer as the amount of time spent at greater depth increased. As DVMs became more established, a fraction of the mesopelagic sound scattering layer ascended upwards to less than 50 m depth, crossing the pycnocline and entering the surface PW layer close to mid-night (Fig. 11b).

The echogram recorded during the *AT800-bio-2* deployment also revealed a persistent mesopelagic scattering layer, typically located below 200 m depth and more than 200 m thick (Fig. 11b). Few sound scattering organisms were detected in in the upper 200 m, as the signal to noise ratio was typically low. However, as during the previous year, thin dense layers of macroplankton were observed within the upper polar water layer. Also, as during the previous year, the centre of mass of the sound scattering layer was shallowest during the early winter and was deepest during early April 2021. During late April 2021 the centre of mass ascended by about 50 m, this ascension coincided with both a reduction in SIF and a reduction in the strength of the slope-current, exhibiting similarities to the ascension observed during July of the previous year.

4. Discussion

The data presented in this paper reveal in unprecedented detail the temporal evolution in the concentration and vertical distribution of macrozooplankton and fish in the northern Barents Sea and on its northern shelf slope. The two moorings in the northern Barents Sea (*M1* and *M5*) were in regions dominated by cold and fresh PW and seasonal sea ice cover, but also significantly influenced by an inflow of wPW (PW

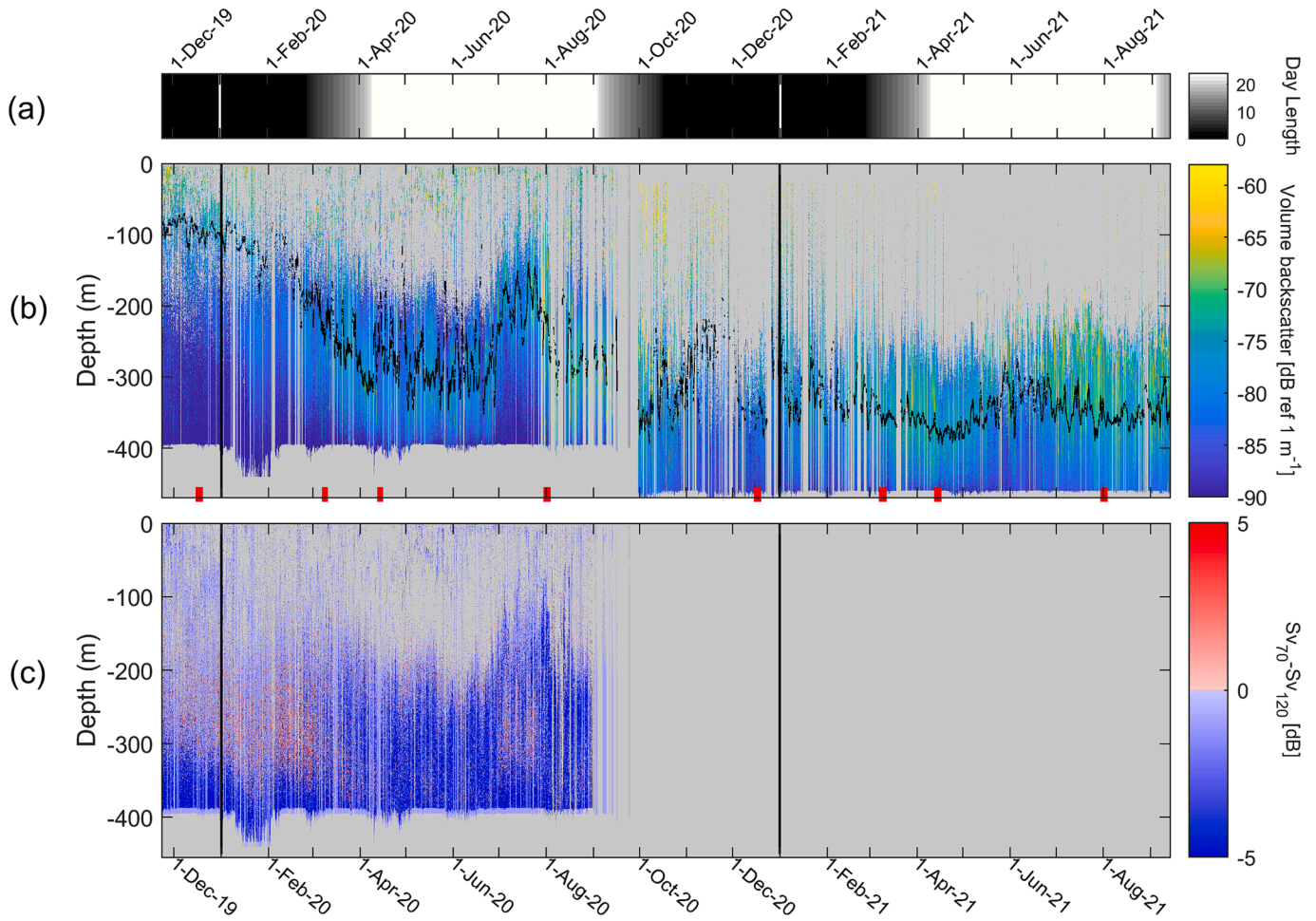

Fig. 10. Timeseries at *AT800* of (a) number of hours the sun is above the horizon each day and (b) echogram of 70 kHz volume backscatter (S_v), where the solid black line indicates the weighted mean depth. The red marks at the bottom of figure b indicate the periods shown in the five-day duration echograms presented in Fig. 11, (c) difference in volume backscatter (S_v at 70 kHz minus S_v at 120 kHz), where red indicates bins where Sv is greater at 70 kHz (fish-like scatterers), and blue indicates bins where S_V is greater at 200 kHz (zooplankton-like scatterers).

mixed with AW) at depth. *AT800* on the northern continental slope was influenced by variability in the AWBC and sea ice conditions. At each mooring site we observed considerable temporal variability in the density distribution of pelagic fish and macrozooplankton over sub-daily to seasonal time scales. Such variability was tightly coupled to changes in hydrographic conditions, with the variable inflow of Atlantic influenced water, and sea ice concentration, being key drivers. The depth of the boundary between the water masses, water temperature, and day length also influenced the vertical distribution of organisms. While descriptive in nature, this study provides the groundwork for future research focused on elucidating the biophysical interactions driving temporal and spatial pattens in fish and macrozooplankton distributions in the Barents Sea, with applications to other Arctic shelf-seas.

4.1. Biophysical interactions

M5-bio on the Great Bank was located in a biologically active region, with high densities of pelagic macrozooplankton, and particularly during 2021 also fish, present throughout most of the year (Fig. 3e and Fig. 4). A recent study (Van Engeland et al., 2023) reveals that this location is dominated by the presence of Arctic zooplankton. Despite the prevailing north-eastward currents recorded at *M5-bio*, PW is more commonly observed at this location than the Atlantic influenced water typically observed to the southwest of the site. This could be due to the local topography, or possibly the existence of an anticyclonic gyre on the Great Bank, similar to that previously described by Quadfasel et al. (1992) and Ivanov and Tuzov, (2021) on the Central Bank. The presence of such a gyre may lead to the retention of biological material over the bank, as observed in other similar gyre systems (e.g. Lough and Manning, 2001; Mohn et al., 2002). This may be one reason for the high density of macroplankton and pelagic fish observed at this site. Particularly high densities of both macrozooplankton and fish were present throughout the winter of 2021–22, with an above average density of scatterers also observed during the winter of 2020–21 (Fig. 7). Full-depth DVM's were observed at *M5-bio* during all seasons except mid-summer, continuing throughout the winter under the ice (Fig. 8). Thus, our data demonstrate the persistent presence of an active (vertically migrating) macrozooplankton community on Great Bank throughout the winter months. This result supports the findings of Berge et al. (2015), who suggested that biomass and biological interactions across most trophic levels in the Barents Sea during the polar night are higher in winter than previously thought.

Observed concentrations of macrozooplankton and fish at *M5-bio* were higher during 2021 than during 2020. The higher near-bottom water temperatures and reduced sea ice concentration during 2021 (Fig. 3) may be possible explanations for this. Another explanation may be the shorter duration over which the water column was vertically mixed during the spring and early summer of 2021 as compared to the previous year. At both *M5-bio* and *M1-bio*, below average densities of macrozooplankton were observed when the water column was vertically

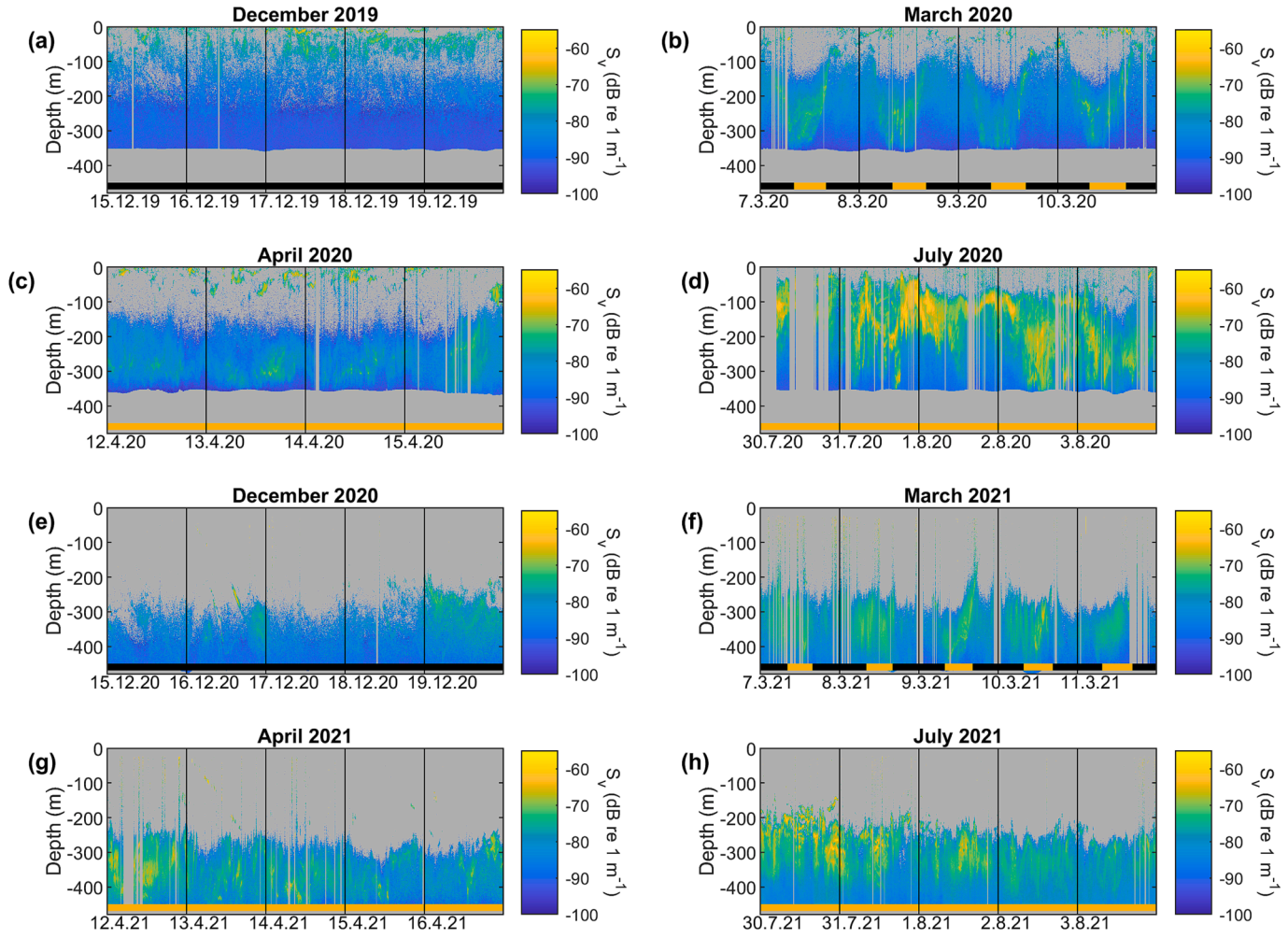

Fig. 11. A comparison of five-day duration echograms of 70 kHz volume backscatter during different seasons extracted from the *AT800-bio* echograms, in (a-d) data are from the *A800-bio-1* mooring and in (e-f) data are from the *AT800-bio-2* mooring. The duration the sun is above the horizon (yellow bars) and below the horizon (black bars) is indicated at the bottom of each figure.

mixed (or at *M1-bio* when the top-to-bottom density difference was minimal), during the spring and early summer. At *M5-bio* the density of pelagic macrozooplankton declined rapidly after the pycnocline descended below the echosounder depth. We note, however, that DVMs exceeding tens of meters in vertical extent were not observed in our data when the water column was vertically mixed. It is possible that zooplankton hide near the bottom during periods of active vertical mixing, either to avoid being carried up to the surface or because food is mixed downwards, negating the need for vertical migrations. This is an important consideration when interpreting the echograms; part of the reason for the apparent decline in the density of macrozooplankton when only one water mass was present may be that many organisms remained below the depth visible to the echo sounder, rather than that they disappeared from the region.

The presence and depth of the pycnocline greatly influenced both the vertical distribution and DVM behaviour of macrozooplankton and fish. The echograms from *M5-bio* commonly reveal multiple scattering layers performing synchronous DVMs which differed in vertical extent and type (nocturnal, inverse and twilight migrations were all observed). For some organisms residing near the seabed or surface, the pycnocline formed a barrier to DVMs, while other organisms migrated upwards through the pycnocline into the overlying water mass. Yet other groups of scatterers resided within the pycnocline and performed daily migrations either upwards or downwards. Species-specific DVM strategies have been reported previously by Jephson and Carlsson, (2009). This study, together with that of Jephson and Carlsson, (2009) reveals the complexity in the physical structuring of the pelagic ecosystem.

At *M1-bio* in the Kvitøya Trough, temporal variability in the area backscattering coefficient was positively correlated to the volume of wPW present at the site. The presence of wPW was itself related to the strength of the transport of Atlantic-influenced water masses through the Kvitøya Trough from the north. A stronger along-slope current and an increased inflow of wPW were associated with a higher concentration of sound scattering organisms at *M1-bio*. Our data reveal a persistent southward depth-averaged flow out of the Kvitøya Trough between mid-summer and early spring of the following year, the strength of which varied considerably over seasonal and synoptic time scales. This is consistent with Lundesgaard et al. (2022) who similarly describe a seasonal cycle characterised by intensified inflows in autumn and early winter, modulated on shorter timescales by wind. Our data also reveal a sustained although relatively weak reversal in the current direction during the late spring and early summer of each year. During this reversal the current direction at *M1-bio* was towards the mouth of the Kvitøya Trough, the volume of wPW decreased or disappeared completely, and the density of sound scattering organisms exhibited a marked decline. It is notable, however, that despite the higher concentration of sound scattering organisms during periods of increased wPW inflow, the highest concentrations of sound scattering organisms throughout the winter months were located within the pycnocline and in the upper, cold PW layer. Conversely, during summer, the highest

density of organisms was observed close to the depth of the pycnocline and within the underlying wPW.

At *AT800-bio* seasonality in the strength of the shelf edge current was the main driver of temporal variability in the local hydrography, with stronger along-slope transport associated with a thickening of the warm core of the AWBC. Previous authors report a stronger inflow and a broader and warmer AW core north of Kvitøya from late autumn into early winter (Renner et al., 2018; Lundesgaard et al., 2022), and our results are consistent with these observations. As a fraction of the Atlantic influenced water transported along the shelf edge intrudes into the Kvitøya Trough, conditions in the AWBC also influence conditions at *M1,* explaining some of the similarity between these sites. However, while a relationship exists between the concentration of sound scattering organisms and the volume of wPW at *M1*, no such relationship was discerned between the along-slope current strength and the concentration of sound scattering organisms at *AT800*. This may be partly because our observations do not span the entire water column. Considering the rapid increase in macrozooplankton following disappearance of the ice in July 2020, it seems likely, as the AWBC is almost absent at this location during July 2020 (Fig. 9d), that seasonality in local production is more significant than seasonality in the advection of organisms by the AWBC. Previous studies in the Fram Strait have reported a relationship between positive temperature anomalies caused by the Atlantic Water transport and increasing contributions of Atlantic copepod species to the zooplankton communities (Gluchowska et al., 2017) and the diversity of gelatinous zooplankton in early summer (Mańko et al., 2020). Atlantic Water inflow likely also influences biodiversity at *AT800*, if not the concentration of sound scattering organisms present. The mean depth of the mesopelagic sound scattering layer at *AT800* shows a seasonal variability driven by changing light conditions (typically deepening during spring as daylight hours increase and shallowing in autumn as daylight hours decrease). The temporary shallowing of the mesopelagic sound scattering layer following the disappearance of the sea ice during summer may be a response to light shading by phytoplankton, following a post-melt phytoplankton bloom.

4.2. Comparison to midwater ring net samples

In this study of biophysical interactions, we discuss observations of volume backscatter without attempting to discriminate groups of organisms beyond fish and macrozooplankton. However, the zooplankton and fish communities in the northern Barents Sea are dominated by a small number of species. The two species of schooling fish in the northern Barents Sea are capelin and polar cod. The reported seasonal distribution of polar cod is such that they may occur at *M1-bio* from June to September and at *M5-bio* throughout the year (Aune et al., 2021). Capelin are widespread throughout the Barents Sea during summer with the main distribution area in the central parts of the Barents Sea, east of Svalbard (Gjøsæter, 1998). During winter capelin remain south of the Polar Front and the ice edge. Both polar cod and capelin may pass *M5-bio* during spawning migrations. Fish schools observed at *M5-bio* during winter, concentrated between 100 and 120 m depth are therefore likely to be polar cod. Fish schools observed during the late spring and autumn, may be either one of these species. The area east of Svalbard where mooring *M1* is located has been suggested as a possible spawning area for polar cod, which spawn under the ice in winter-spring months (Eriksen et al., 2019). High density echoes recorded under the ice during winter at M1 may potentially be spawning polar cod.

A limited number of macrozooplankton net samples, described by Van Engeland et al. (2023) were collected 53 km north-northwest of *M5* (station *P2;* see Fig. 1), 114 km east of M1 in the channel between the Kvitøya and Franz-Victoria Troughs (station *P4*) and at *AT800 (P6),* during our study period. Net samples were collected in August and December 2019 and in March and May 2021 using a Midwater Ring Net (commonly referred to as MIK net) with a ~ 1600 μm mesh size. Vertical hauls were conducted from 10 m above the bottom at *P2* and from 1000 m depth at *AT800*. These data, reproduced from Van Engeland et al. (2023), are presented here in Fig. 12. The data provide some insight into the community of larger zooplankton present in the northern Barents Sea during our study period. Samples collected north-northeast of M5 at *P2* revealed a dominance of Arctic biota (Van Engeland et al., 2023). Copepods contributed during all seasons, particularly August when they made up more than 50 % of the total biomass, while amphipods comprised more than 70 % of the total biomass in December 2021, having made up a minor contribution to the biomass during the other sampling periods (Fig. 12). Gelatinous zooplankton and pteropods made up the largest biomass fractions in March and May 2021 respectively. Total biomass concentration at *P2* was greatest in December 2019 and low during March and May 2021. High abundance of planktic foraminifera was also found at P2 in December 2019 (Zamelczyk et al., 2021), but absent in March 2021 (Anglada-Ortiz et al., 2023). Thus, these studies support our observations of high macrozooplankton biomass during winter in this region, and further suggest that amphipods and pteropods contribute significantly to the high density of macrozooplankton observed on the Great Bank during winter (2020–21).

Copepods, particularly Arctic species, contribute significantly to the mesozooplankton biomass in the Barents Sea in all seasons and many previous authors (e.g. Tande, 1989; Aarflot, et al., 2018) have demonstrated the key role played by copepods in the transferal of energy to higher trophic levels. While the larger *C. hyperboreus* (on average 8 mm) can be detected at the frequency range used in this study, smaller mesoplankton including smaller copepods are difficult to detect in our data set given the limited frequency range. This is a recognised limitation of our study and may partly explain the relatively low density of macroplankton recorded in the echograms from M5 in August 2021 considering the high biomass fraction of copepods reported in the same area by Van Engeland et al. (2023).

At *AT800* (*P6*), a mixture of temperate species, deep-water species, and sympagic amphipods were reported by Van Engeland et al. (2023). Gelatinous zooplankton comprised more than 50 % of the total biomass obtained by the MIK net during all seasons, with chaetognaths, classified separately, dominating this group. Copepods also comprised a significant fraction (>0.2) of the biomass during all seasons, with the larger C. hyperboreus contributing to 50 % or more (Van Engeland et al., 2023). Amphipods and euphausiids contributed little to the total zooplankton biomass. The total biomass concentration obtained from the MIK net was greater during August 2019, than during the other months sampled, consistent with our observations of a peak in macrozooplankton density following disappearance of the ice in late summer.

4.3. Seasonal progression

Primary production in the Arctic is strongly pulsed over the short productive spring and summer (Dalpadado et al., 2020) and the timing of the phytoplankton bloom is strongly dependent on sea ice conditions. Our study period spans two years with quite different regional sea ice conditions: during the winter and spring of 2020 sea ice cover was close to the long-term average and ice was present at our mooring sites until relatively late in the summer. In 2021 the sea ice extent was considerably lower and below the long-term average (although still higher than most of the years during the 2012–2016 period). Chlorophyll data recorded at 26 m depth at *M1-phys* (not shown) reveals the presence of algal biomass between early May and late October 2021, indicating a potential food source for herbivorous zooplankton well into the autumn. While our data reveal a rapid increase in the density of the pelagic sound scattering layer following ice melt at the two northern most stations, the duration and intensity of this increase differed between years. During 2020, a short but intense peak occurred following the later disappearance of the sea ice, lasting approximately one month. During 2021, the peak was longer in duration and began earlier in the year, suggesting that the seasonal progression of macrozooplankton mirrors that of phytoplankton. Stations M1 and M5 exhibited some similarities in

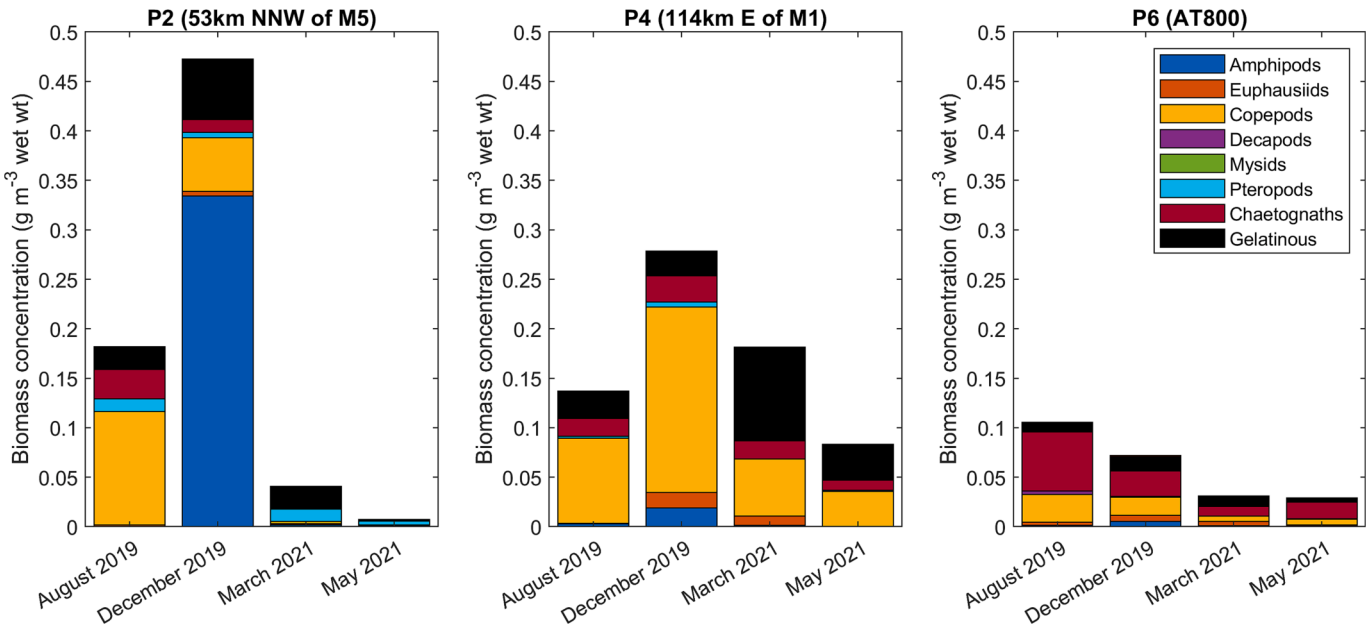

Fig. 12. Biomass concentration for the major taxon groups collected by midwater ring net hauls conducted during different seasons at stations P2, P4 and P6 (locations indicated in Fig. 1). Data are reproduced from Van Engeland et al. (2023).

seasonal progression. At both stations, relatively high densities of sound scattering organisms were observed from late summer through until late winter or early spring, with low densities during the spring and early summer. As there is no primary production during the Arctic winter, we assume the high density of macrozooplankton observed during the winter months is due to the presence of carnivores feeding on a store of lipid rich herbivores, possibly alongside detritus feeders. This is consistent with the conclusions of Kohlbach et al. (2021) and Kunisch et al. (2023) who describe the northern Barents Sea macrozooplankton community as undergoing a seasonal cycle with strong omnivorous or carnivorous feeding in winter and primarily herbivory in summer.

4.4. *Limitations and future perspectives*

Like all acoustic studies, this study is limited by the presence of acoustic blind zones close to the bottom and surface. The bottom mounted instruments at *M1-bio* and *M5-bio* recorded data from approximately 9 m to 14 m above the seabed due to the height of the mooring apparatus and a 2 m blanking distance above the transducer. This is a limitation of upward facing instruments and explains why we regularly observed sound scattering layers descending below the depth range of the echosounders when undertaking DVMs. Upward looking transducers are limited in how close to the surface they can effectively measure by surface waves, sea ice and air bubbles mixed down by diving predators, as well as by passing marine traffic. During calm weather we were typically able to obtain data within 2 m of the ocean surface at *M1-bio* and *M5-bio* (an advantage of upward facing echosounders over shipboard instruments). At *AT800-bio*, interpretation of the data was impacted by the limited range of the echosounder. A further limitation of this study was the lack of calibrated echosounder data at *M1-bio* and during the second deployment at *AT800*. While the uncalibrated data only allowed observation of the relative changes in the density distribution of organisms during individual mooring deployments, we believe the data give valuable insight into the temporal processes and seasonality at these sites.

The taxonomic composition of the sound scattering organisms recorded by the Signature100s is likely to vary considerably both seasonally and between stations (due to differences in latitude, depth, and regional hydrography). Improved understanding of such taxonomic diversity is essential to interpreting trophic interactions. Despite the narrow frequency range of the Signature100 (70 kHz–120 kHz) the work of Cutter et al. (2022) has demonstrated the potential of supervised learning to isolate individual species (krill), however this requires knowledge of the length distribution of the organisms. While the lack of supporting net samples is a hinderance to such classification, previous studies in the region may allow classification at least to a group level. A more detailed analysis of acoustic target types is intended as the subject of a future paper. Trophic links between specific species are believed to be weak in Arctic systems and identifying organisms to group level may be sufficient to interpret food web interactions. Such analyses would provide insight into the consequences of the Atlantification of the northern Barents Sea for the seasonal succession in food web structure and functioning, predator breeding and foraging success, and ultimately inform ecosystem-based fishery management.

In this work we comment only briefly on observations of DVMs. We note the existence of DVMs at all stations, and on the Great Bank during all seasons except mid-summer. We also note the complexity in the structure of observed DVM's and the role of DVM is providing a link between organisms residing within different water masses. The importance of species specific DVMs to the structuring of pelagic food webs and for biochemical cycling and carbon export has been highlighted by several recent papers (Bandara et al., 2021) and references therein). We therefore believe a more detailed analysis of the DVM events in the data presented here is merited, and this is also intended to be the subject of a following paper.

5. Summary and conclusions

As part of the Nansen Legacy projects observational programme, moored multi-frequency echo-sounders have been deployed along-side moorings collecting a range of physical and chemical data at three locations in the northern Barents Sea. Considered together, the data from these moorings have provided an unprecedented opportunity to observe seasonally varying biophysical interactions in this seasonally ice-covered region. Data collected over a period of approximately two years reveal significant variability in the density, thickness and depth distribution of macrozooplankton and fish within the epipelagic and meso-pelagic realms, over time scales ranging from diurnal to seasonal.

A close relationship is demonstrated between the physical environment (sea ice conditions, prevailing currents, and hydrography) and the concentration and vertical distribution of pelagic organisms. This study highlights the tight relationship between the physical characteristics of the pelagic environment and the organisms that live there.

The density of large zooplankton and pelagic fish on the Great Bank was greatest during autumn and winter. In the Kvitøya Trough, the highest density of zooplankton and fish was observed during the late summer and early autumn, with high densities also observed during the winter months. By contrast, during the spring and early summer, the density of pelagic sound scattering organisms was relatively low at both stations. Hence the data presented in this study highlight the persistent presence of a macrozooplankton community, undertaking diel vertical migrations, in the northern Barents Sea throughout the winter months. Our data also demonstrate the existence of a thick and persistent mesopelagic sound scattering layer in the Atlantic Water boundary current of the northern shelf-slope. The thickness and density of this layer, which rises into the epipelagic during July, are influenced by surface irradiance and sea ice conditions but show no relationship to the strength of the shelf-edge current.

Water mass distribution was identified as one of the most important structuring factors influencing the vertical distribution of macrozooplankton and fish. The relative volumes of PW and wPW present at the mooring sites and the way in which these water masses were layered vertically exerted a dominant control on both the seasonal and shorter-term variability in the density distribution of sound scattering organisms on the northern Barents Sea shelf (on the Great Bank and in the Kvitøya Trough). The highest concentration of pelagic organisms was typically observed when both wPW and PW layers were present, resulting in a stratified water column. An increased inflow of wPW was typically associated with an increase in the depth integrated density of sound scattering organisms. However, in the Kvitøya Trough a higher concentration of organisms was observed within the upper PW layer during the winter months, while the underlying AW layer remained relatively empty. Synoptic scale changes in the density distribution of sound scattering organisms were on occasion of similar magnitude to the seasonal variability, particularly on the Great Bank.

Small scale DVMs were observed at all three stations throughout the entire year, with full depth DVMs observed at the more southerly *M5* station during all seasons except mid-summer. At the more northerly stations, the vertical range of DVMs and the density of the sound scattering layers performing migrations was greatest during the transition between the polar night and midnight sun periods. The vertical depth range of DVMs was adjusted daily in response to changes in environmental conditions. Water column structure exerted a control on the depth range of DVM's with some organisms migrating within a particular water mass and others crossing the pycnocline into a different water mass. Our data provide examples of nocturnal migration, reverse migration and twilight migrations often at the same time, with up to three distinct scattering layers performing synchronous but differing migrations. This study highlights the complex layering and interactions of pelagic organisms distributed throughout the water column and the environmental/physical factors which influence this.

Declaration of competing interest

The authors declare the following financial interests/personal relationships which may be considered as potential competing interests: Heather Cannaby reports financial support was provided by Institute of Marine Research.

Data availability

Data will be made available on request.

Acknowledgements

The research was performed within the frame-work of the Nansen Legacy project (RCN-276730), funded by the Research Council of Norway, Norway. This study also utilised data collected within the A-TWAIN (Fram Centre project 66050), SIOS InfraNor (RCN 269927) and INTAROS (EU H2020 contract no. 727890) projects. This study made use of E.U. Copernicus Marine Service Information (https://doi.org/10.48670/moi-00165).

Appendix A. Supplementary material

Supplementary data to this article can be found online at https://doi.org/10.1016/j.pocean.2023.103159.

References

Aarflot, J.M., Skjoldal, H.R., Dalpadado, P., Skern-Mauritzen, M., 2018. Contribution of *Calanus* species to the mesozooplankton biomass in the Barents Sea. ICES J. Mar. Sci. 75 (7), 2342–2354. https://doi.org/10.1093/icesjms/fsx221.

Aksenov, Y., Bacon, S., Coward, A.C., Nurser, G., 2010. The North Atlantic inflow to the Arctic Ocean: high-resolution model study. J. Mar. Syst. 79 (1), 1–22.

Anglada-Ortiz, G., Meilland, J., Ziveri, P., Chierici, M., Fransson, A., Jones, E., Lander Rasmussen, T., 2023. Seasonality of marine calcifiers in the northern Barents Sea: spatiotemporal distribution of planktic foraminifera and shelled pteropods and their contribution to carbon dynamics. Prog. Oceanogr. 218, 103121.

Zamelczyk, K., Fransson, A., Chierici, M., Jones, E., Meilland, J., Anglada-Ortiz, G., Lødemel, H.H., 2021. Distribution and Abundances of Planktic Foraminifera and Shelled Pteropods During the Polar Night in the Sea-Ice Covered Northern Barents Sea. Front. Mar. Sci. 8, 644094. https://doi.org/10.3389/fmars.2021.644094.

Asbjørnsen, H., Årthun, M., Skagseth, Ø., Eldevik, T., 2020. Mechanisms underlying recent Arctic Atlantification. Geophys. Res. Lett. 47 (15), e2020GL088036. doi: 10.1029/2020GL088036.

Aune, M., Raskhozheva, E., Andrade, H., Augustine, S., Bambulyak, A., Camus, L., Carroll, J., Dolgov, A. V., Hop, H., Moiseev, D., Renaud, P.E., Varpe, Ø., 2021. Distribution and ecology of polar cod (*Boreogadus saida*) in the eastern Barents Sea: a review of historical literature. Mar. Environ. Res. 166, 105262, ISSN 0141-1136.

Bandara, K., Varpe, Ø., Wijewardene, L., Tverberg, V., Eiane, K., 2021. Two hundred years of zooplankton vertical migration research. Biol. Rev. 96 (4), 1547–1589.

Basedow, S.L., Sundfjord, A., von Appen, W.-J., Halvorsen, E., Kwasniewski, S., Reigstad, M., 2018. Seasonal Variation in Transport of Zooplankton Into the Arctic Basin Through the Atlantic Gateway, Fram Strait. Front. Mar. Sci. 5, 194. https://doi.org/10.3389/fmars.2018.00194.

Berge, J., Cottier, F., Last, K.S., Varpe, Ø., Leu, E., Søreide, J., Eiane, K., Falk-Petersen, S., Willis, K., Nygård, H., Vogedes, D., Griffiths, C., Johnsen, G., Lorentzen, D., Brierley, A.S., 2009. Diel vertical migration of Arctic zooplankton during the polar night. Biol. Lett. 569, 72. https://doi.org/10.1098/rsbl.2008.0484.

Berge, J., Daase, M., Renaud, P.E., Ambrose, W.G., Darnis, G., Last, K.S., Leu, E., Cohen, J.H., Johnsen, G., Moline, M.A., Cottier, F., Varpe, Ø., Shunatova, N., Bałazy, P., Morata, N., Massabuau, J.-C., Falk-Petersen, S., Kosobokova, K., Hoppe, C.J.M., Węsławski, J.M., Kukliński, P., Legeżyńska, J., Nikishina, D., Cusa, M., Kędra, M., Włodarska-Kowalczuk, M., Vogedes, D., Camus, L., Tran, D., Michaud, E., Gabrielsen, T.M., Granovitch, A., Gonchar, A., Krapp, R., Callesen, T.A., 2015. Unexpected levels of biological activity during the polar night offer new perspectives on a warming Arctic. Curr. Biol. 25 (19), 2555–2561.

Boyer, T.P., Garcia, H.E., Locarnini, R.A., Zweng, M.M., Mishonov, A.V., Reagan, J.R., Weathers, K.A., Baranova, O.K., Seidov, D., Smolyar, I.V., 2018. World Ocean Atlas 2018. [temperature]. NOAA National Centers for Environmental Information. Dataset. https://www.ncei.noaa.gov/archive/accession/NCEI-WOA18. Accessed 16 March 2023.

Brierley, A.S., Saunders, R.A., Bone, D.G., Murphy, E.J., Enderlein, P., Conti, S.G., et al., 2006. Use of moored acoustic instruments to measure short-term variability in abundance of Antarctic krill. Limnol. Oceanogr. Methods 4 (2), 18–29. https://doi.org/10.4319/lom.2006.

Cutter Jr, G.R., Reiss, C.S., Nylund, S., Watters, G.M., 2022. Antarctic krill biomass and flux measured using wideband echosounders and acoustic Doppler current profilers on submerged moorings. Front. Mar. Sci. 9 (784469) https://doi.org/10.3389/fmars.2022.784469.

Dalpadado, P., Arrigo, K.R., Van Dijken, G.L., Skjoldal, H.R., Bagøien, E., Dolgov, A.V., Prokopchuk, I.P., Sperfeld E., 2020. Climate effects on temporal and spatial dynamics of phytoplankton and zooplankton in the Barents Sea. Prog. Oceanogr. 185, 102320. ISSN 0079-6611. doi: 10.1016/j.pocean.2020.102320.

Dalpadado, P., Ingvaldsen, R.B., Stige, L.C., Bogstad, B., Knutsen, T., Ottersen, G., Ellertsen, B., 2012. Climate effects on Barents Sea ecosystem dynamics. ICES J. Mar. Sci. 69 (7), 1303–1316. https://doi.org/10.1093/icesjms/fss063.

Dolgov, A.V., Johannsen, E., Bogstad, B., 2021. The Barents Sea – Ecosystem, Resources, Management. Half a century of Russian-Norwegian cooperation. In: Jakobsen, T., Ozhigin, V. (Eds.), An Overview of Trophic Interactions in the Barents Sea Publisher, Tapir Academic Press, Chapter: 8.1, pp. 431–436.

Egbert, G.D., Erofeeva, S.A., 2002. Efficient inverse modeling of barotropic ocean tides. J. Atmos. Oceanic Tech. 19 (2), 183–204.

Eriksen, E., Huserbråten, M., Gjøsæter, H., Vikebø, F., Albretsen, J., 2019. Polar cod eggs and larval drift pattern in the Svalbard archipelago. Polar Biol. 43, 1029–1042. https://doi.org/10.1007/s00300-019-02549-6.

Ershova, E.A., Kosobokova, K.N., Banas, N.S., Ellingsen, I., Niehoff, B., Hildebrandt, N., Hirche, H.J., 2021. Sea ice decline drives biogeographical shifts of key *Calanus* species in the central Arctic Ocean. Glob. Chang. Biol. 27 (10), 2128–2143. https://doi.org/10.1111/gcb.15562.

Fossheim, M., Primicerio, R., Johannesen, E., Ingvaldsen, R.B., Aschan, M.M., Dolgov, A. V., 2015. Recent warming leads to a rapid borealization of fish communities in the Arctic. Nat. Clim. Chang. 5, 673–677. https://doi.org/10.1038/nclimate2647.

Frainer, A., Primicerio, R., Kortsch, S., Aune, M., Dolgov, A.V., Fossheim, M., Aschan, M. M., 2017. Climate-driven changes in functional biogeography of Arctic marine fish communities. PNAS 114 (46), 12202–12207. https://doi.org/10.1073/pnas.1706080114.

Gjøsæter, H., 1998. The population biology and exploitation of capelin (*Mallotus villosus*) in the Barents Sea. Sarsia 83 (6), 453–496. https://doi.org/10.1080/00364827.1998.10420445.

Gjøsæter, H., Wiebe, P.H., Knutsen, T., Ingvaldsen, R.B., 2017. Evidence of diel vertical migration of mesopelagic sound-scattering organisms in the Arctic. Front. Mar. Sci. 4 (332) https://doi.org/10.3389/fmars.2017.00332.

Gluchowska, M., Dalpadado, P., Beszczynska-Möller, A., Olszewska, A., Ingvaldsen, R.B., Kwasniewski, S., 2017. Interannual zooplankton variability in the main pathways of the Atlantic water flow into the Arctic Ocean (Fram Strait and Barents Sea branches). ICES Journal of Marine Science 74 (7), 1921–1936. https://doi.org/10.1093/icesjms/fsx033.

Grémillet, D., Fort, J., Amélineau, F., Zakharova, E., Le Bot, T., Sala, E., Gavrilo, M., 2015. Arctic warming: nonlinear impacts of sea-ice and glacier melt on seabird foraging. Global Change Biology 21 (3), 1116–1123. https://doi.org/10.1111/gcb.12811.

Hays, G.C., 2003. A review of the adaptive significance and ecosystem consequences of zooplankton diel vertical migrations. Hydrobiologia 503, 163–170. https://doi.org/10.1023/B:HYDR.0000008476.23617.b0.

ICES, 2021. The Working Group on the Integrated Assessments of the Barents Sea (WGIBAR). ICES Sci. Reports 3, 236. https://doi.org/10.17895/ices.pub.8241 *Diversity and seasonal development of large zooplankton along physical gradients in the Arctic Barents Sea.* Available from: https://www.researchgate.net/publication/371644661_Diversity_and_seasonal_development_of_large_zooplankton_along_physical_gradients_in_the_Arctic_Barents_Sea#fullTextFileContent [accessed Nov 13 2023].

Ingvaldsen, R.I., Loeng, H., 2009. Physical oceanography. In: Sakshaug, E., Johnsen, G., Kovacs, K. (Eds.), Ecosystem Barents Sea, Tapir Academic Press, Trondheim, Norway, pp. 33–64, 587 pp.

Ivanov, V.V., Tuzov, F.K., 2021. Formation of dense water dome over the Central Bank under conditions of reduced ice cover in the Barents Sea. Deep Sea Res. Part I: Oceanogr. Res. Pap. 175, 103590. ISSN 0967-0637. doi: 10.1016/j.dsr.2021.103590.

Irigoien, X., Klevjer, T., Røstad, A., et al., 2014. Large mesopelagic fishes biomass and trophic efficiency in the open ocean. Nat Commun 5, 3271. https://doi.org/10.1038/ncomms4271.

Jephson, T., Carlsson, P., 2009. Species- and stratification-dependent diel vertical migration behaviour of three dinoflagellate species in a laboratory study. Journal of Plankton Research 31 (11), 1353–1362. https://doi.org/10.1093/plankt/fbp078.

Ji, R., Edwards, M., Mackas, D.L., Runge, J.A., Thomas, A.C., 2010. Marine plankton phenology and life history in a changing climate: current research and future directions. Journal of Plankton Research 32 (10), 1355–1368. https://doi.org/10.1093/plankt/fbq062.

Kohlbach, D., Schmidt, K., Hop, H., Wold, A., Al-Habahbeh, A.K., Belt, S.T., Woll, M., Graeve, M., Smik, L., Atkinson, A., Assmy, P., 2021. Winter carnivory and diapause counteract the reliance on ice algae by Barents Sea zooplankton. Front. Mar. Sci. 8, 640050 https://doi.org/10.3389/fmars.2021.640050.

Kortsch, S., Primicerio, R., Aschan, M., Lind, S., Dolgov, AV, Planque, B., 2019. Food-web structure varies along environmental gradients in ahigh-latitude marine ecosystem. Ecography 42, 295–308.

Kortsch, S., Rrimicerio, R., Fossheim, M., Dolgov, A., Aschan, M., 2015. Climate change alters the structure of arctic marine food webs due to poleward shifts of boreal generalists. Proc. R. Soc. B. 282, 20151546.

Kraft, A., Berge, J., Varpe, Ø., Stig, F.-P., 2013. Feeding in Arctic darkness: mid-winter diet of the pelagic amphipods *Themisto abyssorum* and *T. libellula*. Mar. Biol. 160, 241–248. https://doi.org/10.1007/s00227-012-2065-8.

Kunisch, E.H., Graeve, M., Grandinger, R., Flores, H., Varpe, Ø., Bluhm, B.A., 2023. What we do in the dark: prevalence of omnivorous feeding activity in Arctic zooplankton during polar night. Limnol. Oceanogr. 9999, 1–7.

Lee, K., Mukai, T., Kang, D., Iida, K., 2004. Application of acoustic doppler current profiler combined with a scientific echo sounder for krill *euphausia pacifica* density estimation. Fish. Sci. 70 (6), 1051–1060.

Leu, E., Wiktor, J., Søreide, J.E., Berge, J., Falk-Petersen, S., 2010. Increased irradiance reduces food quality of sea ice algae. Mar Ecol Prog Ser 411, 49–60.

Levine, R.M., De Robertis, A., Grunbaum, D., Wilson, C.D., 2023. Transport-driven seasonal abundance of pelagic fishes in the Chukchi Sea observed with seafloor-mounted echosounders. ICES Journal of Marine Science 80 (4), 987–1001. https://doi.org/10.1093/icesjms/fsad024.

Lewis, K.M., Van Dijken, G.L., Arrigo, K.R., 2020. Changes in phytoplankton concentration now drive increased Arctic Ocean primary production. Science 369 (6500), 198–202.

Lind, S., Ingvaldsen, R.B., 2012. Variability and impacts of Atlantic Water entering the Barents Sea from the north. Deep Sea Research I 62, 70–88.

Lind, S., Ingvaldsen, R.B., Furevik, T., 2016. Arctic layer salinity controls heat loss from deep Atlantic layer in seasonally ice-covered areas of the Barents Sea. Geophys. Res. Lett. 43 (10), 5233–5242. https://doi.org/10.1002/2016GL068421.

Lind, S., Ingvaldsen, R.B., Furevik, T., 2018. Arctic warming hotspot in the northern Barents Sea linked to declining sea-ice import. Nat. Clim. Chang. 8, 634–639. https://doi.org/10.1038/s41558-018-0205-y.

Loeng, H., 1991. Features of the physical oceanographic conditions of the Barents Sea. Polar Res. 10 (1), 5–18. https://doi.org/10.3402/polar.v10i1.6723.

Lough, R.G., Manning, J.P., 2001. Tidal-front entrainment and retention of fish larvae on the southern flank of Georges Bank. Deep Sea Res. Part II 48 (1–3), 631–644.

Lundesgaard, Ø., Sundfjord, A., Lind, S., Nilsen, F., Renner, A.H.H., 2022. Import of Atlantic Water and sea ice controls the ocean environment in the northern Barents Sea. Ocean Sci. 18, 1389–1418. https://doi.org/10.5194/os-18-1389-2022.

Maclennan, D.M., Fernandes, P.G., Dalen, J., 2002. A consistent approach to definitions and symbols in fisheries acoustics, ICES. Journal of Marine Science 59 (2), 365–369. https://doi.org/10.1006/jmsc.2001.1158.

Mańko, M.K., Gluchowska, M., 2020. Footprints of Atlantification in the vertical distribution and diversity of gelatinous zooplankton in the Fram Strait (Arctic Ocean). Prog. Oceanogr. 189, 102414. https://doi.org/10.1016/j.pocean.2020.102414.

Matishov, G.G., Matishov, D.G., Moiseev, D.V., 2009. Inflow of Atlantic-origin Waters to the Barents Sea along Glacial Troughs. Oceanologia 51 (3), 321–340.

Mohn, C., Bartsch, J., Meincke, J., 2002. Observations of the mass and flow field at Porcupine Bank. ICES J. Mar. Sci. 59 (2), 380–392. https://doi.org/10.1006/jmsc.2001.1174.

Oziel, L., Sirven, J., Gascard, J.C., 2016. The Barents Sea frontal zones and water masses variability (1980–2011). Ocean Sci. 12(1), 169–184. doi: 10.5194/os-12-169-2016.

Pnyushkov, A.V., Polyakov, I.V., Ivanov, V.V., Aksenov, Y., Coward, A.C., Janout, M., Rabe, B., 2015. Structure and variability of the boundary current in the Eurasian Basin of the Arctic Ocean. Deep Sea Res. Part I 101, 80–97. https://doi.org/10.1016/j.dsr.2015.03.001.

Quadfasel, D., Rudels, B., Selchow, S., 1992. The Central Bank vortex in the Barents Sea: water mass transformation and circulation. ICES Mar. Sci. Symp. 195.

Renner, A.H.H., Sundfjord, A., Janout, M.A., Ingvaldsen, R.B., Beszczynska-Moller, A., Pickart, R.S., Perez-Hernandez, M.D., 2018. Variability and redistribution of heat in the Atlantic water boundary current north of Svalbard. J. Geophys. Res. Oceans 123 (9), 6373–6391. https://doi.org/10.1029/2018JC013814.

Ressler, P.H., Dalpadado, P., Macaulay, G.J., Handegard, N., Skern-Mauritzen, M., 2015. Acoustic surveys of euphausiids and models of baleen whale distribution in the Barents Sea. Mar Ecol Prog Ser 527, 13–29. https://doi.org/10.3354/meps11257.

Sandø, A.B., Nilsen, J.E.Ø., Gao, Y., Lohmann, K., 2010. The importance of heat transport and local air-sea heat fluxes for Barents Sea climate variability. J. Geophys. Res. 115 (C7), 1–11. https://doi.org/10.1029/2009JC005884.

Skjoldal, H.R., Eriksen, E., Gjøsæter, H., 2022. Size-fractioned zooplankton biomass in the Barents Sea: Spatial patterns and temporal variations during three decades of warming and strong fluctuations of the capelin stock (1989–2020), Prog. Oceanogr. 206, 102852. ISSN 0079-6611.

Smedsrud, L.H., Lars, H., Esau, I., Ingvaldsen, R.I., Eldevik, T., Haugan, P.M., Li, C., Lien, V.S., Olsen, A., Omar, A.M., Otterå, O.H., Risebrobakken, B., Sandø, A.B., Semenov, V.A., Sorokina, S.A., 2013. The role of the Barents Sea in the Arctic climate system. Rev. Geophys. 51 (7), 415–449. https://doi.org/10.1002/rog.20017.

Sundfjord, A., Assmann, K.M., Lundesgaard, Ø., Renner, A.H.H., Lind, S., Ingvaldsen, R. B., 2020. Suggested water mass definitions for the central and northern Barents Sea, and the adjacent Nansen Basin: Workshop Report. The Nansen Legacy Report Series 8/2020. doi: 10.7557/nlrs.5707.

Tande, K.S., 1989. *Calanus* in North Norwegian fjords and in the Barents Sea. In Sakshaug, E., Hopkins, C.C.E and Øritsland, N.A. (eds.): Proceedings of the Pro Mare Symposium on Polar Marine Ecology, Trondheim 12-16 May 1990. Polar Research 10(2): 389-407.

Våge, K., Pickart, R.S., Pavlov, V., Lin, P., Torres, D.J., Ingvaldsen, R., Sundfjord, A., Proshutinsky, A., 2016. The Atlantic Water Boundary Current in the Nansen Basin: Transport and Mechanisms of Lateral Exchange. J. Geophys. Res. Oceans 121 (9), 6946–6960. https://doi.org/10.1002/2016JC011715.

Van Engeland, T., Bagøien, E., Wold, A., Cannaby, H.A., Majaneva, S., Vader, A., Rønning, J., Handegard, N.O., Klevjer, T.A., Dalpadado, P., Ingvaldsen, R.B., 2023. Macrozooplankton diversity and seasonal development along physical gradients in the Arctic Barents Sea. Phys. Oceanogr. 206 (7), 103065.

Velasco, D.W., Nylund, S., Pettersen, T., 2018. Combined current profiling and biological echosounding results from a single ADCP. OCEANS MTS/IEEE 1–5. https://doi.org/10.1109/OCEANSKOBE.2018.8559356.